Randomized-MLP Regularization Improves Domain Adaptation and Interpretability in DINOv2

Joel Valdivia Ortega [1,2,3,*] **Lorenz Lamm** [1,3,4] **Franziska Eckardt** [5]

Benedikt Schworm [5] **Marion Jasnin** [2,6,*] **Tingying Peng** [1,*]

[1]Helmholtz AI, Helmholtz Munich, Neuherberg, Germany
[2]Helmholtz Pioneer Campus, Helmholtz Munich, Neuherberg, Germany
[3]School of Computation, Information and Technology, TUM, Garching, Germany
[4]Biozentrum, University of Basel, Basel, Switzerland
[5]Department of Ophthalmology, LMU University Hospital, LMU Munich, Munich, Germany
[6]Department of Chemistry, TUM, Garching, Germany.

{joel.valdiviaortega, lorenz.lamm,
marion.jasnin, tingying.peng}@helmholtz-munich.de
{franziska.eckardt,benedikt.schworm}@med.uni-muenchen.de

Abstract

Vision Transformers (ViTs), such as DINOv2, achieve strong performance across domains but often repurpose low-informative patch tokens in ways that reduce the interpretability of attention and feature maps. This challenge is especially evident in medical imaging, where domain shifts can degrade both performance and transparency. In this paper, we introduce Randomized-MLP (RMLP) regularization, a contrastive learning-based method that encourages more semantically aligned representations. We use RMLPs when fine-tuning DINOv2 to both medical and natural image modalities, showing that it improves or maintains downstream performance while producing more interpretable attention maps. We also provide a mathematical analysis of RMLPs, offering insights into its role in enhancing ViT-based models and advancing our understanding of contrastive learning.[1]

1 Introduction

Learning robust visual representations remains a central challenge in computer vision. Transformer-based models, such as Vision Transformers (ViTs) [11], have emerged as powerful backbones, especially when trained with self-supervised methods like contrastive or reconstruction-based learning [30, 5, 15, 32, 20]. These approaches yield generalizable models, which can be fine-tuned for specialized tasks, particularly in domains with limited labeled data, like medical and biological imaging [21, 19, 8, 25].

However, despite their empirical success, ViTs exhibit persistent issues in how they encode and distribute semantic information. Previous studies have observed that large ViTs often store global context within semantically weak or background regions [41, 38, 9]. These structural artifacts can

*Corresponding authors

[1]Code and pre-trained models are available at `https://github.com/peng-lab/rmlp`.

39th Conference on Neural Information Processing Systems (NeurIPS 2025).

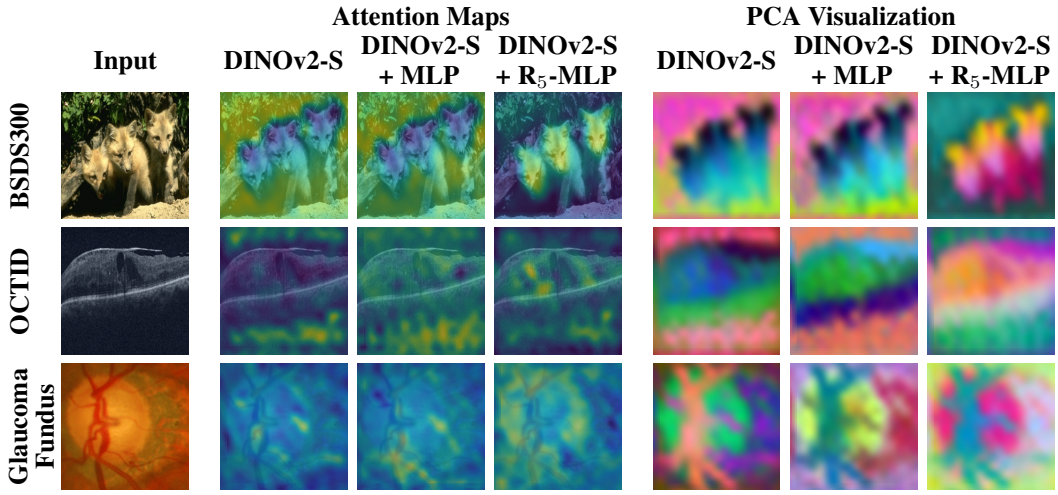

Figure 1: **Left:** Input image from BSDS300 [27], OCTID [14] and Glaucoma Fundus [2] datasets from top to bottom. **Middle:** Second- (BSDS300) and first-order (OCTID/Glaucoma Fundus) attention maps (see Section 1) over grayscale image. **Right:** Visualizations of top-3 PCA of patch tokens using DINOv2-S, DINOv2 fine-tuned on selected modality, and DINOv2 fine-tuned on selected modality using our regularizer. Colors are assigned in the RGB regime as the norm of the principal components. More qualitative results are available in Appendix A.1.

degrade performance on dense prediction tasks and compromise interpretability, a critical concern in biomedical domains [16, 46].

Our analysis reveals that these artifacts are not limited to large ViTs. Even though the small variant of DINOv2 [30] performs well on natural image tasks (Table 1), it still exhibits anomalous attention behavior. In medical imaging, DINOv2-S struggles to generalize to dense tasks such as segmentation (Table 2), despite achieving strong performance on classification tasks (Table 3a). This supports the hypothesis that it sacrifices local detail in favor of encoding global information through uninformative tokens. By analyzing patch token norms and their principal components, we identify *first-order artifacts*—where high-norm tokens align with background regions in ophthalmological images—and *second-order artifacts*—where the variance captured by the top three principal components is misaligned with semantic relevance in natural images (Figure 1). First order artifacts are more pronounced in medical images, where DINOv2-S statistically attends more to void or anatomically irrelevant regions than to biologically meaningful tissue (Table 4a).

To address these issues, we propose the *Randomized Multi-Layer Perceptron* (RMLP), a lightweight, theory-driven regularization module that improves semantic alignment in ViT representations. RMLP is motivated by the geometry of contrastive learning [5, 35] and enhances interpretability without requiring retraining or architectural changes. When applied to DINOv2, RMLP yields significant improvements in both natural and biomedical domains, achieving state-of-the-art classification and segmentation performance on ophthalmology datasets with minimal computational overhead. Additionally, we demonstrate that RMLP generalizes beyond DINOv2 by fine-tuning SwAV [4]—a model trained under a different self-supervised paradigm— and showing it consistently improves performance across modalities, indicating the broader applicability of our approach.

2 Related Work

Artifacts in Transformer Representations. Transformers are known to exhibit uneven attention allocation across input tokens. In NLP, Xiao, et al. [41] showed that early-position tokens receive disproportionate attention, regardless of their semantic importance. Sun, et al. [38] attributed such behavior to sparse, high-norm activations. Extending these observations to vision, Darcet, et al. [9] found that ViTs often produce a small set of high-norm patch tokens concentrated in background regions, which act as "registers" for global context. While these patch repurposing have been mostly studied in large-scale ViTs, our work shows it also emerge in smaller models like DINOv2-S.

Mitigating Attention Artifacts. Prior attempts to address attention artifacts have focused on heuristic or architectural solutions. Darcet, et al. [9] proposed adding learnable tokens and retraining the model on proprietary datasets. Jiang, et al. [18] showed that even untrained tokens can mitigate high-norm anomalies by absorbing excess activation. Others introduced auxiliary loss terms [40] or attention-smoothing modules [42] to encourage more uniform feature distributions. While these methods show empirical improvements, they lack theoretical grounding, require expensive retraining, or cannot be used as domain adaptation techniques. In contrast, our proposed RMLP module is easy to integrate, requires no retraining, and is grounded in the geometry of contrastive representation spaces. It also improves both semantic fidelity and interpretability across modalities.

3 Randomized-Multi-Layer Perceptron (RMLP)

Central to our approach is the observation that the structure of the representation heads—namely, the DINO [5] and iBOT [44] heads—play a key role in how information is encoded across patch and class tokens. In DINOv2, the contrastive framework aligns student and teacher global representations via the DINO head (operating on the class token), while the iBOT head introduces masked image modeling by aligning patch tokens through a cross-entropy objective. Both heads are implemented as MLPs.

Building on the findings of Darcet, et al. [9], we hypothesize that the representation heads are a key enabler of this behavior. To counteract this, we replace the learnable MLP heads with a randomized, non-trainable operator designed to preserve the topology of the representation space. This encourages the backbone to learn more robust and interpretable features, while preventing the heads from exploiting token-level classification shortcuts.

To avoid modifying the architecture, we first express the structure of the DINO and iBOT heads. A standard MLP [30] can be written as $f = \phi_r \circ \alpha_{r-1} \circ \cdots \circ \alpha_1 \circ \phi_1$, where ϕ_i are linear layers and α_i activations. We replace each ϕ_i with a randomized map $\varphi_i : \mathbb{R}^m \to \mathbb{R}^n$ as

$$\varphi_i((x_1, \ldots, x_m)) = (x_1, \ldots, x_n) + \Gamma_i(x_1, \ldots, x_m)^\top, \tag{1}$$

where $(x_1, \ldots, x_n)$ can be a truncated or zero-padded version of the input vector, $\Gamma_i \in \mathbb{R}^{n \times m}$ is a Gaussian matrix with i.i.d. entries drawn from $\mathcal{N}(0, \lambda/n)$ and λ is a tunable *amplitude*. This operator can also be seen as a residual connection. Thus, we formally define an R_λ-MLP as

$$g = \varphi_r \circ \alpha_{r-1} \circ \cdots \circ \alpha_1 \circ \varphi_1. \tag{2}$$

RMLPs introduce no trainable parameters, yet remain fully compatible with end-to-end contrastive training objectives like DINO [5] and iBOT [44].

4 Theoretical Analysis

We now develop a topological framework to analyze how ViT embeddings evolve while passing through transformer blocks (Theorem 1), the way it generalizes from its training data into a bigger domain (Theorem 2 and Corollary 3) and how our RMLP regularizer impacts the contrastive learning paradigm (Theorem 4). This enables the characterization of RMLPs as random operators which turn point embeddings into *probability balls* (Corollary 5), improving robustness and promoting sparcity without altering the topology of learned representations when an adequate amplitude is chosen.

Theorem 1. *Let Ω be an image space and Ψ a latent space. A ViT $\mathcal{V} : \Omega \to \Psi$ can be decomposed as a tokenization function $\mathcal{C} : \Omega \to \Psi$ followed by a sequence of transformer blocks $T : \Psi \to \Psi$, which are defined by local orthonormal bases generated in the attention heads by the queries, keys, and values layers along with the input data itself.*

Proof. ViTs use the attention mechanism to decompose the data using queries and keys layers, creating a field that data follows during the representation process. The value layers act as embeddings within the space defined by queries and keys. For a complete proof, refer to Theorem 11 in Appendix A.2. □

Training with the KoLeo regularizer [35] ensures that $\mathcal{V}$ remains injective since the loss, namely,

$$\mathcal{L}_{\text{KoLeo}}\left(\{x_1, \ldots, x_n\}\right) = -\frac{1}{n} \sum_{i=1}^{n} \log\left(\min_{j \neq i} \|x_i - x_j\|_2\right)$$

would diverge otherwise. Continuity of $\mathcal{C}$, along with KoLeo and augmentations, guarantees that T is locally injective (see Def. 6) on $\mathcal{C}[\Omega]$. These properties allow T to generalize from its training data into Ψ while preserving its embedding ability as shown in Corollary 3.

Theorem 2. *Being an homeomorphism an invertible continuous function with continuous inverse, assuming T is locally injective and taking Ψ to be a metric space, there exists $\varepsilon > 0$ such that T is an homeomorphism on $\{x \in \Psi : \delta(x, \mathcal{C}[\Omega]) < \varepsilon\}$, where δ is the distance on Ψ.*

Proof. T is continuous from Theorem 1. Since images can only take values from a finite set, Ω is bounded and by construction, $\mathcal{C}$ is continuous. Further, taking the codomain of $\mathcal{C}$ as a metric space and using again that images take discrete values, we can assume $\mathcal{C}[\Omega]$ is compact because of being a finite union of closed sets, namely singletons of images. Thus, for Lemma 12 in Appendix A.2, an $\varepsilon > 0$ exists such that T is injective in $\{x \in \Psi : \delta(x, \mathcal{C}[\Omega]) < \varepsilon\}$, i.e., is invertible in that subset. Furthermore, since Ψ is metric, the result follows from Lemma 13 in Appendix A.2. □

Corollary 3. *If $\mathcal{A} \subseteq \Omega$ is the training data, and T is locally injective on $\mathcal{A}$, the following holds:*

- *) There exists $\varepsilon > 0$ such that T is an homeomorphism on an ε-cloud containing $\mathcal{A}$ (see Def. 7).*
- *) Let $P, Q \subseteq \Omega$. $\mathcal{C}[P] \cup \mathcal{C}[Q]$ is disconnected in Ψ if and only if $\mathcal{V}[P] \cup \mathcal{V}[Q]$ is disconnected in Ψ (see Def. 8), which can contribute to the batch effect.*
- *) If $D \subseteq \Psi$ is dense in Ψ (see Def. 9), then $\mathcal{V}[D]$ is dense in $\mathcal{V}[\Psi]$.*

Proof. A complete proof is in Appendix A.2 in Theorem 18. □

Theorem 4. *Let $\{p_1, \ldots, p_N\} \subseteq \mathbb{R}^m$, $\varepsilon > 0$, and $\lambda > 0$, with Γ a matrix of size $n \times m$ with i.i.d. normal entries $\mathcal{N}(0, \lambda n^{-1})$. Then, for each $x \in \mathbb{R}^m$, $\mathbb{E}[\|\Gamma x\|_2^2] = m\lambda n^{-1}\|x\|_2^2$. Moreover, Γ produces an ε-distortion (see Def. 14) on the set $E = \left\{ \frac{p_i - p_j}{\|p_i - p_j\|} : 1 \leqslant i < j \leqslant N \right\}$ with high probability if*

$$\lambda n^{-1} < \frac{\varepsilon^2}{8 \ln N}.$$

Proof. (*Sketch*) Using concentration results for Gaussian matrices, we follow [28]. A complete proof can be found at Appendix A.2 in Theorem 19. □

Corollary 5. *If $E = \{x_1, \ldots, x_N\} \subseteq \mathbb{S}^{m-1}$, $\varepsilon > 0$, and $\varphi : \mathbb{R}^m \to \mathbb{R}^n$ is defined as in Eq. 1 with $\lambda n^{-1} < \varepsilon^2/(8 \ln N)$, then for all $i \in \{1, \ldots, N\}$,*

$$\|(x_{i,1}, \ldots, x_{i,n}) - \varphi(x_i)\|_2 < \varepsilon$$

with high probability.

Proof. This follows directly from the definition of φ and Theorem 4. □

We now analyze the impact of RMLP heads on image embeddings. Let us take an RMLP g as in Equation 2 with amplitude λ and GELU activation acting on the embedding $\mathcal{V}(x) = ((z_{i,j})_{j \leqslant d})_{i \leqslant \nu}$. Applying Corollary 5, the first random layer φ_1 turns each token z_i into a ball of radius ε, determined by the embedding's dimension, λ, and the number of tokens ν.

By Theorem 4, the output of $\varphi_1(\mathcal{V}(x))$ lies on a sphere of radius $d\lambda n_1^{-1}$ on expectation. The contrastive losses encourage similarity between views, while the KoLeo regularizer promotes injectivity. However, the GELU activation restricts the space to a spherical region with mostly positive coordinates, where dispersion is optimized via approximate orthogonality among embeddings. Successive layers $\varphi_2, \varphi_3, \varphi_4$ expand the radius of probability balls further. Thus, $g \circ \mathcal{V}(x)$ becomes a point cloud creating a probability ball, rather than individual points, regularizing the learning by applying cross-entropy over neighborhoods. If the RMLP amplitude λ is too large, the topology of the embedding space may be distorted, as shown in Figure 2. Remarkably, the topological properties of ViTs remain unaffected whether MLPs or RMLPs heads are used during training, as our analysis is independent of it.

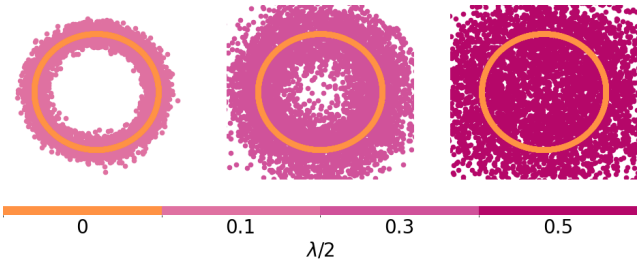

Figure 2: Visualization of a randomized operator following Equation 1, applied to the unit circle in $\mathbb{R}^2$ ($\lambda/2 = 0$) for different values of λ. For $\lambda/2 = 0.1$, the point cloud retains a circular structure, preserving the topology of the circle. For $\lambda/2 = 0.5$, the point cloud no longer exhibits a circular topology, as it transitions to a disk-like shape.

5 Implementation and Training Details

Model Variants. We use two ViT-based self-supervised models: DINOv2-S [30] and SwAV [4]. Fine-tuned variants include standard MLP heads and our regularized version using R_λ-MLP. Fine-tuning follows the DINOv2 protocol with the original head architecture retained. Hyperparameters and external code can be found in Tables 5, 6.

Training Modalities. Each backbone is fine-tuned separately on three modalities: ImageNet-1k (natural), Colour Fundus Photography (CFP), and Optical Coherence Tomography (OCT) (Table 7a). Medical datasets are sourced from public subsets aggregated in RETFound [43], ensuring geographic diversity (Table 7b).

Hybrid Architecture for Dense Tasks. For pixel-level predictions, we pair the ViT encoder with a UNet-style decoder [33, 17]. Patch and class tokens are projected and fused with early UNet features, enabling multi-scale feature integration. This ViT-UNet hybrid is used for segmentation and depth estimation tasks.

6 Experimental Setting

Evaluation Setup. We fine-tune DINOv2-S and SwAV with R_λ-MLP at amplitudes $\{0.1, 5, 10, 20\}$, running 10 trials per modality and setting. Baselines use MLP heads. Downstream tasks employ either linear probes or the hybrid decoder depending on task type. Results are averaged over runs and tested for significance using the Mann–Whitney U test [26], appropriate under our distributional assumptions. Qualitative results for both natural and ophthalmological modalities can be found in Appendix A.1.

Natural Image Tasks. On ImageNet-1k [34], we perform image classification training with cross-entropy. For semantic segmentation of [45] and depth estimation of [36], we apply a linear head and the ViT-UNet hybrid. Segmentation is trained with a linear combination of focal [23] and dice loss [29]. Depth maps are rescaled to [0, 50] and trained with focal loss. Table 1 reports performance compared to baselines [9, 40, 42].

OCT and CFP Tasks. We assess disease classification and retinal layer segmentation. Segmentations emphasize the ophthalmologically relevant Outer Nuclear Layer (ONL). UNet output biases are initialized (-2 for background, 2 for others) for stable training. We benchmark against RETFound [43] and a domain-specific model [12] (Tables 2, 3).

Cross-Modal Attention Analysis. We visualize attention maps across modalities: second-order for natural images [27] and first-order for OCT [14] and CFP [2]. High vs. low-information patches are separated using a 2-component Gaussian Mixture Model on smoothed gradient at patch level.

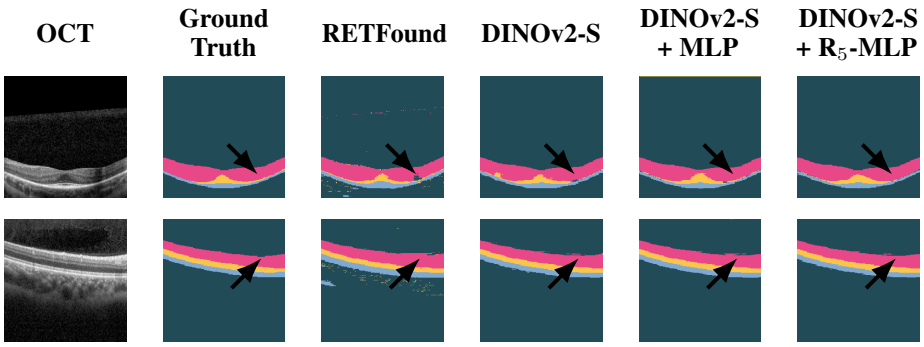

Figure 3: Semantic segmentation of retinal layers on the dataset from Eckardt, et al. [12] (OCT) using different backbones (columns) in a ViT-UNet hybrid. Black arrows highlight cases where fine-tuning DINOv2-S with R_5-MLP outperforms other models.

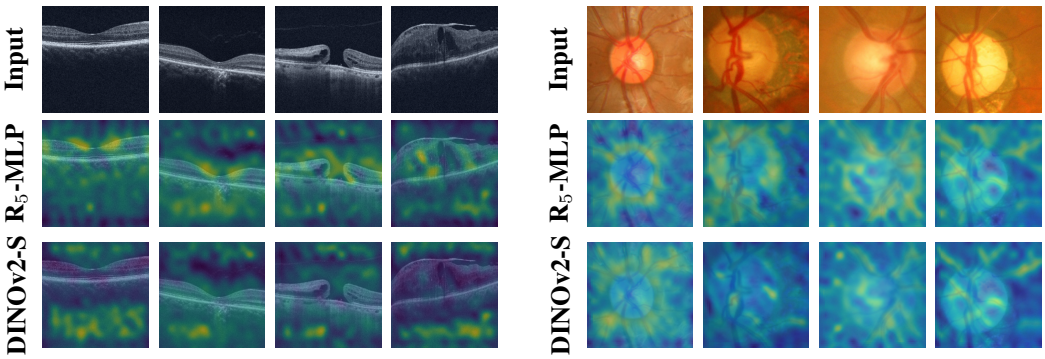

Figure 4: **Top**: OCTID [14] (left) and Glaucoma Fundus [2] (right) images. **Middle**: First-order attention maps from model fine-tuned with R_5-MLP overlaid on grayscale version of input image. **Bottom**: First-order attention maps from DINOv2-S overlaid on grayscale version of input image. Brighter maps indicate more attention. While DINOv2-S focuses on void regions, DINOv2-S with R_5-MLP attends to key anatomical features in the OCTs—such as the foveal pit, macular hole, and epithelial detachment—and highlights the rim and blood vessels in Fundus images.

7 Results and Discussion

Effectiveness of RMLP Regularization. Across natural and medical image domains, fine-tuning with R_λ-MLP consistently outperforms MLP baselines. On natural images, it better preserves performance compared to other regularizers. In the medical domain, despite limited data and single-GPU training, R_λ-MLP achieves state-of-the-art OCT segmentation (Figure 3) and improves classification, especially with 1-NN, indicating enhanced representation quality (Table 3). While linear-head classification with R_λ-MLP slightly trails state-of-the-art or DINOv2-S, this reflects differing latent space structures since RMLPs promote neighborhood-based similarity (Theorem 4, Corollary 5), whereas MLPs enforce linear separability. Larger λ values degrade performance by altering representation topology (Tables 1–3, Figure 2), while smaller amplitude values do not consistently improve downstream results, highlighting a tradeoff between retaining information and preserving topological structure ViTs need to overcome during fine-tuning.

Enhancement on Cross-Paradigm Learning. RMLPs enable effective adaptation of models trained under different learning paradigms, such as SwAV [4], when combined with DINOv2 learning algorithm (Tables 2b, 3b,). While applying DINOv2 to standard MLPs also yields gains, RMLPs consistently deliver superior performance across tasks.

Table 1: Performance across downstream tasks on natural images. Semantic segmentation on ADE20k [45], depth estimation on NYU-Depth V2 [36] and image classification on ImageNet-1k [34]. Bold indicates best mean, † second-best on for each base model (DINOv2-S, DINOv2-G and SwAV). Underlined values are significantly better than DINOv2-S ($p < 0.001$); * and *** denote significance over base model fine-tuned with MLP at $p < 0.1$ and $p < 0.001$ (Mann–Whitney U test [26]). Results show mean±std from ten independently fine-tuned backbones.

Model	Semantic Segmentation ↑		Depth Estimation ↓		Image Classification ↑		
	ViT-UNet Hybrid	Linear Head	ViT-UNet Hybrid	Linear Head	1-Nearest Neighbor	Random Forest	Linear Head
	DINOv2-S						
DINOv2-S [30]	**0.81±0.1**	†0.76±0.1*	**7±3*****	**9±3*****	**0.70*****	**0.18*****	**0.77±0.01*****
DINOv2-S + MLP	0.78±0.1	0.75±0.1	†8±3	†10±3	0.64±0.01	0.14±0.01	0.73±0.01
DINOv2-S + $R_{0.1}$-MLP	0.61±0.1	0.66±0.1	8±1	9±1	0.64±0.01	0.15±0.01	0.74±0.06
DINOv2-S + R_5-MLP	†0.80±0.1***	**0.77±0.1*****	**7±3*****	**9±3*****	†0.65±0.01***	†0.16±0.01***	†0.76±0.01***
DINOv2-S + R_{10}-MLP	†0.80±0.1***	**0.77±0.1*****	**7±3*****	**9±3*****	†0.65±0.01***	0.15±0.01***	**0.77±0.01*****
DINOv2-S + R_{20}-MLP	†0.76±0.2	**0.77±0.1*****	**7±3*****	**9±3*****	0.64±0.01***	0.14±0.01***	0.75±0.01***
Registers [9]	0.72±0.2	0.67±0.1	7±1	9±1	0.28	0.05	0.74±0.01**
DVT [42]	0.45±0.2	0.64±0.01	7±1	9±1	**0.7**	0.11	0.64±0.01
	DINOv2-G						
Sinder [40]	0.51±0.2	0.56±0.1	6±3	8±1	0.78	0.12	†0.76±0.01***
	SwAV						
SwAV [4]	**0.37±0.1**	–	**12±1**	–	–	–	**0.69±0.01**
SwAV + MLP	0.29±0.08	–	†13±1	–	–	–	**0.69±0.01**
SwAV + R_5-MLP	0.34±0.09	–	†13±2	–	–	–	**0.69±0.01**
SwAV + R_{10}-MLP	0.27±0.1	–	**12±1**	–	–	–	**0.69±0.01**
SwAV + R_{20}-MLP	†0.36±0.1	–	†13±1	–	–	–	**0.69±0.01**

Table 2: Performance metrics for semantic segmentation on Eckardt, et al. [12] dataset using a ViT-UNet hybrid. Results show mean±std of DICE scores from ten independently fine-tuned backbones using DINOv2 and SwAV as base models. Bold numbers indicate best performance, † the second-best, and underlined results outperform RETFound (p < 0.001, Mann-Whitney U test). Statistical significance vs. base model fine-tuned with MLP is shown by * (p < 0.1).

(a) Base model: DINOv2.

Model	Averaged DICE	DICE on ONL
RETFound [43]	0.92±0.06	0.59±0.10
Registers [9]	0.92±0.1	0.62±0.21
Sinder [40]	0.90±0.21	0.61±0.2
DVT [42]	0.78±0.25	0.43±0.22
DINOv2-S [30]	0.79±0.20	0.54±0.20
DINOv2 + MLP	0.86±0.20	0.55±0.20
DINOv2 + $R_{0.1}$-MLP	†0.94±0.12	†0.68±0.21
DINOv2 + R_5-MLP	**0.97±0.03***	**0.72±0.09***
DINOv2 + R_{10}-MLP	0.87±0.20	0.61±0.20
DINOv2 + R_{20}-MLP	0.70±0.30	0.47±0.20
Eckardt, et al. [12]	0.92±0.03	0.44±0.03

(b) Base model: SwAV.

Model	Averaged DICE	DICE on ONL
SwAV [4]	†0.89±0.15	0.59±0.14
SwAV + MLP	0.88±0.15	†0.6±0.18
SwAV + $R_{0.1}$-MLP	**0.92±0.12**	**0.64±0.1**
SwAV + R_5-MLP	0.83±0.27	0.58±0.2
SwAV + R_{10}-MLP	0.71±0.33	0.42±0.23
SwAV + R_{20}-MLP	0.84±0.26	0.58±0.21

Attention Artifacts on Natural Images. Fine-tuning on ImageNet-1k slightly reduces the CorLoc score for both MLP and RMLP heads (Table 4b), a minor drop consistent with other regularization methods and attributable to fine-tuning rather than the RMLPs. While regularized models from literture maintain global context and classification accuracy comparable to DINOv2-S, they degrade patch token quality in dense prediction tasks (Table 1). Notably, DINOv2-S encodes global information in patch tokens from low-information regions, a tendency amplified by regularized models. Fine-tuning with MLPs or RMLPs reduces this artifact, equalizing patch token behavior, with RMLPs better preserving downstream performance post fine-tuning (Table 4).

Table 3: Performance metrics for pathology classification across OCT and CFP modalities. Results show mean±std from ten independently fine-tuned backbones. Bold numbers indicate best performance, † the second-best, and underlined results outperform RETFound ($p < 0.001$, Mann-Whitney U test). Statistical significance vs. base model fine-tuned with MLP is shown by * ($p < 0.1$), ** ($p < 0.01$), and *** ($p < 0.001$).

(a) Accuracy for pathology classification using DINOv2-S as base model.

Dataset		DINOv2-S [30]	DINOv2-S + MLP	DINOv2-S + $R_{0.1}$-MLP	DINOv2-S + R_5-MLP	DINOv2-S + R_{10}-MLP	DINOv2-S + R_{20}-MLP
		1-Nearest Neighbor classification					
OCTID [14]	(0.8)	†0.75***	0.69±0.02	0.68±0.01	**0.78±0.01*****	0.73±0.01***	0.68±0.01***
Glaucoma Fundus [2]	(0.78)	0.67***	0.64±0.01	0.65±0.01	**0.71±0.09*****	†0.69±0.09***	0.63±0.07
IDRID [31]	(0.44)	0.42***	0.43±0.03	0.36±0.01	**0.47±0.01*****	†0.44±0.02***	0.43±0.04*
JSIEC [7]	(0.45)	0.59***	0.51±0.02	0.51±0.01	**0.67±0.01*****	†0.65±0.07***	0.59±0.08***
MESSIDOR-2 [1, 10]	(0.56)	†0.53***	0.47±0.01	0.43±0.01	**0.55±0.01*****	†0.53±0.08***	0.52±0.08***
PAPILA [22]	(0.63)	†0.71***	0.65±0.03	0.65±0.01	**0.74±0.02*****	†0.71±0.01***	0.65±0.03**
Retina [6]	(0.5)	0.54	0.54±0.02	0.39±0.01	**0.58±0.01*****	**0.58±0.01*****	†0.57±0.01***
		Random Forest classification					
OCTID [14]	(0.81)	**0.75*****	0.54±0.01	0.58±0.01	†0.74±0.01***	0.73±0.02***	0.69±0.02***
Glaucoma Fundus [2]	(0.73)	**0.69*****	0.65±0.08	0.67±0.01	†0.68±0.08***	0.67±0.08**	†0.68±0.09**
IDRID [31]	(0.4)	†0.49***	0.46±0.01	0.47±0.01	0.47±0.01***	0.46±0.01**	**0.5±0.05*****
JSIEC [7]	(0.28)	0.28***	0.26±0.08	0.25±0.01	**0.32±0.08*****	†0.29±0.06***	0.28±0.06***
MESSIDOR-2 [1, 10]	(0.58)	**0.58**	**0.58±0.01**	0.58±0.01	**0.58±0.01*****	**0.58±0.01*****	**0.58±0.01**
PAPILA [22]	(0.69)	**0.72*****	0.68±0.01	0.68±0.01	†0.71±0.01***	†0.71±0.01***	0.69±0.09**
Retina [6]	(0.59)	**0.59*****	0.55±0.07	0.55±0.01	**0.59±0.07*****	†0.58±0.06***	†0.58±0.08***
		Linear classification					
OCTID [14]	(0.93±0.05)	**0.88±0.08****	0.76±0.02	0.82±0.01	†0.87±0.01***	†0.87±0.01***	0.86±0.01***
Glaucoma Fundus [2]	(0.83±0.06)	**0.79±0.06*****	0.71±0.09	0.73±0.02	0.75±0.01***	0.75±0.01***	†0.76±0.01***
IDRID [31]	(0.44±0.04)	**0.50±0.04****	†0.44±0.03	0.48±0.03	0.42±0.03	0.40±0.03	†0.44±0.03
JSIEC [7]	(0.72±0.01)	0.73±0.07***	0.63±0.01	0.68±0.02	**0.78±0.01*****	†0.76±0.01***	0.73±0.03***
MESSIDOR-2 [1, 10]	(0.56±0.03)	0.46±0.08	†0.52±0.03	0.51±0.04	**0.54±0.07***	†0.52±0.08	0.49±0.09
PAPILA [22]	(0.67±0.07)	**0.71±0.05**	0.66±0.04	0.66±0.03	†0.69±0.03	0.7±0.03	†0.69±0.03
Retina [6]	(0.51±0.03)	0.52±0.04	0.53±0.02	0.51±0.02	†0.54±0.03	†0.54±0.03	**0.55±0.02***

(b) Accuracy for pathology classification using SwAV as base model.

Dataset		SwAV [4]	SwAV+ MLP	SwAV+ $R_{0.1}$-MLP	SwAV+ R_5-MLP	SwAV+ R_{10}-MLP	SwAV+ R_{20}-MLP
OCTID [14]	(0.93±0.05)	**0.84±0.02**	†0.83±0.02	**0.84±0.02**	**0.84±0.02**	0.82±0.02	**0.84±0.02**
Glaucoma Fundus [2]	(0.83±0.06)	**0.76±0.01**	**0.76±0.01**	†0.75±0.01	**0.76±0.01**	**0.76±0.01**	**0.76±0.02**
IDRID [31]	(0.44±0.04)	0.45±0.03	**0.49±0.02**	0.47±0.02	**0.49±0.04**	0.47±0.02	†0.48±0.04
JSIEC [7]	(0.72±0.01)	**0.73±0.01**	†0.72±0.02	†0.72±0.01	**0.73±0.01**	**0.73±0.01**	†0.72±0.01
MESSIDOR-2 [1],[10]	(0.56±0.03)	**0.55±0.04**	**0.55±0.03**	**0.55±0.02**	†0.54±0.02	**0.55±0.02**	**0.55±0.01**
PAPILA [22]	(0.67±0.07)	0.63±0.05	†0.65±0.04	0.62±0.03	**0.66±0.04**	†0.65±0.04	0.64±0.04
Retina [6]	(0.51±0.03)	0.52±0.03	†0.53±0.03	†0.53±0.02	**0.54±0.02**	0.52±0.02	**0.54±0.02**

Attention Artifacts on Ophthalmological Modalities. Both RETFound and DINOv2-S, along with its regularized variants from literature, achieve strong classification accuracy on ophthalmology datasets using patch tokens alone (Table 4c), even from void regions, indicating excessive global information leakage. Moreover, these models exhibit weak or negative correlation with retinal layer presence (Table 4a, Figure 4). In contrast, models fine-tuned with RMLPs (using suitable λ) show better anatomical alignment and reduced attention artifacts as well as better performance in dense tasks (Table 2). This is crucial, as interpretable pathology detection relies on attending to anatomically relevant regions.

ViT-UNet Hybrids. Combining ViT backbones with UNet-style decoders consistently improves performance on dense prediction tasks (Tables 1, 8), highlighting the benefit of integrating global context with local spatial detail.

Table 4: Evaluation of patch tokens repurposing.

(a) Pearson correlation between patch tokens on the top 25% ranked by norm and presence of retinal layers in Eckardt, et al. [12]

Model	Correlation
RETFound [43]	0.0±0.01
Registers [9]	-0.19±0.13
Sinder [40]	0.0±0.17
DVT [42]	-0.37±0.09
DINOv2-S [30]	-0.13±0.14
DINOv2 + MLP	0.19±0.03
DINOv2 + $R_{0.1}$-MLP	0.15±0.02
DINOv2 + R_5-MLP	**0.21±0.03****
DINOv2 + R_{10}-MLP	0.2±0.04
DINOv2 + R_{20}-MLP	0.16±0.01

(b) CorLoc scores applying LOST [37] with default parameters on VOC07 [13] and accuracy on ImageNet-1k using 1-Nearest Neighbors on class tokens and patch tokens of minimum/maximum norm of second-order attention maps from low and high information patches respectively (see Section 1). Bold and underline indicate best and second-best accuracy per model.

Model	CorLoc ↑	Classification accuracy ↑
Registers [9]	35.20	0.71/0.38/0.34
Sinder [40]	**33.97**	**0.78**/0.39/**0.37**
DVT [42]	31.23	0.71/**0.42**/**0.37**
DINOv2-S [30]	34.18	0.71/0.31/0.26
DINOv2-S + MLP	31.18±0.03	0.63±0.01/0.20±0.01/0.18 ±0.01
DINOv2-S + $R_{0.1}$-MLP	31.20±0.04	0.63±0.01/0.20±0.01/0.18 ±0.01
DINOv2-S + R_5-MLP	31.17±0.05	0.64±0.01/0.21±0.01/0.19±0.01
DINOv2-S + R_{10}-MLP	31.17±0.05	0.64±0.01/0.21±0.01/0.19±0.01
DINOv2-S + R_{20}-MLP	31.19±0.07	0.63±0.01/0.20±0.01/0.18±0.01

(c) Pathology classification accuracy on Eckardt, et al. [12], OCTID [14], and aggregated CFP datasets ([2, 31, 7, 1, 10, 22, 6]) using Random Forest with class tokens and patch tokens of minimum/maximum norm from low and high information patches respectively (see Section 1). Bold and underline indicate best and second-best accuracy per model per dataset.

Model	Eckardt, et al. [12]	OCTID [14]	CFP
RETFound [43]	**1.0**/0.92 /0.87	**0.77**/0.45/0.47	**0.53±0.17**/0.51±0.17/0.51±0.17
Registers [9]	0.83/**0.87**/0.86	**0.67**/0.55/0.62	**0.54±0.15**/0.5±0.16/0.5±0.17
Sinder [40]	0.76/**0.8**/0.67	**0.78**/0.56/0.55	**0.54±0.16**/0.5±0.16/0.48±0.17
DVT [42]	0.77/0.7/**0.94**	**0.76**/0.61/0.57	**0.55±0.14**/0.51±0.15/0.52±0.15
DINOv2-S [30]	0.74/**0.84**/0.77	**0.73**/0.48/0.49	**0.55±0.14**/0.49±0.17/0.49±0.18
DINOv2 + MLP	**0.94±0.03**/0.67±0.07/0.86±0.02	**0.55±0.02**/0.36±0.01/0.38±0.01	**0.53±0.15**/0.47±0.17/0.47±0.17
DINOv2-S + $R_{0.1}$-MLP	**0.95±0.02**/0.68±0.08/0.87±0.03	**0.55±0.02**/0.36±0.01/0.38±0.02	**0.53±0.15**/0.47±0.17/0.47±0.17
DINOv2-S + R_5-MLP	**0.96±0.02**/ 0.67±0.07/0.86±0.02	**0.55±0.02**/0.36±0.01/0.37±0.01	**0.53±0.15**/0.47±0.17/0.48±0.17
DINOv2-S + R_{10}-MLP	**0.94±0.02**/0.69±0.08/0.85±0.04	**0.55±0.02**/0.36±0.01/0.38±0.01	**0.53±0.15**/0.47±0.17/0.48±0.17
DINOv2-S + R_{20}-MLP	**0.95±0.02**/0.7±0.07/0.87±0.02	**0.55±0.01**/0.36±0.01/0.37±0.01	**0.53±0.15**/0.47±0.17/0.47±0.17

8 Conclusions

Our work shows that RMLP regularization enhances the interpretability and robustness of ViT representations across both natural and ophthalmological domains. By inducing sparsity in patch tokens and mitigating first- and second-order artifacts, fine-tuning using R_λ-MLPs produces more structured embeddings. Despite being trained on limited data and using small computational resources, R_λ-MLPs help ViTs achieve strong performance in classification and dense prediction tasks both on natural and ophthalmological images. These results highlight randomized-MLPs as a lightweight and effective approach for regularizing representation geometry, pointing to a promising direction for developing more semantically grounded and interpretable vision transformers.

Limitations. The optimal regularization strength may depend on the data modality or the dimensionality of the ViT's latent space. However, this work does not propose a principled method for selecting it, relying instead on heuristic tuning. Additionally, our experiments are currently limited to small- and mid-scale datasets. Future work should investigate performance at larger scales and across a broader range of domains.

Acknowledgments and Disclosure of Funding

J.V.O. and L.L. received support from the Helmholtz Association under the joint research school "Munich School for Data Science - MUDS". T.P and B.S. received support from the DFG grant 513025799. We want to thank Salome Kazeminia and Sophia J. Wagner for the valuable inputs and conversations during the making of this paper.

References

[1] Abràmoff, M. D. et al.: Automated analysis of retinal images for detection of referable diabetic retinopathy. JAMA Ophthalmol. 131, 351–357 (2013).

[2] Ahn, J. M. et al.: A deep learning model for the detection of both advanced and early glaucoma using fundus photography. PLoS ONE 14, e0207982 (2018).

[3] Aptos 2019 blindness detection (2019) Kaggle. Available at: https://www.kaggle.com/competitions/aptos2019-blindness-detection/data (Accessed: 30 April 2025).

[4] Caron, M., Misra, I., Mairal, J., Goyal, P., Bojanowsky, P., Joulin, A.: Unsupervised Learning of Visual Features by Contrastive Cluster Assignments. NeurIPS. arXiv:2006.09882v5 (2021)

[5] Caron, M., Touvron, H., Misra, I., Jégou, H., Mairal, J., Bojanowski, P., and Joulin, A.: Emerging properties in self-supervised vision transformers. ICCV (2021).

[6] Cataract dataset (2019) Kaggle. Available at: https://www.kaggle.com/competitions/aptos2019-blindness-detection/data (Accessed: 30 April 2025).

[7] Cen, L.-P. et al.: Automatic detection of 39 fundus diseases and conditions in retinal photographs using deep neural networks. Nat. Commun. 12, 4828 (2021).

[8] Chen, C., et al.: MA-SAM: Modality-agnostic SAM Adaptation for 3D Medical Image Segmentation. arXiv. arXiv:2309.08842 (2024)

[9] Darcet, T., Oquab, M., Mairal, J., Bojanowski, P.: Vision transformers need registers. arXiv. arXiv:2309.16588 (2024)

[10] Decencière, E. et al.: Feedback on a publicly distributed image database: the Messidor database. Image Anal. Stereol. 33, 231–234 (2014).

[11] Dosovitskiy, A., Beyer, L., Kolesnikov, A., Weissenborn, D., Zhai, X., Unterthiner, T., Dehghani, M., Minderer, M., Heigold, G., Gelly, S., et al.: An image is worth 16x16 words: Transformers for image recognition at scale. arXiv preprint arXiv:2010.11929 (2020)

[12] Eckardt, F., Mittas, R., et al.: Deep Learning-Based Retinal Layer Segmentation in Optical Coherence Tomography Scans of Patients with Inherited Retinal Diseases. Klin Monbl Augenheilkd. doi: 10.1055/a-2227-3742 (2024)

[13] Everingham, M., Van Gool, L., Williams, C.K.I. et al.: The PASCAL Visual Object Classes (VOC) Challenge. Int J Comput Vis 88, 303–338. https://doi.org/10.1007/s11263-009-0275-4 (2010)

[14] Gholami, P. et al.: OCTID: optical coherence tomography image database. Comput. Electr. Eng. 81, 106532 (2020)

[15] He, K. et al.: MAE: Masked Autoencoders Are Scalable Vision Learners. CVPR. arXiv:2111.06377 (2022)

[16] Huang, H., Zou, J., Meng, L., Yue, X., Zhao, Q., Li, J., Song, C., Jimenez, G., Li, S., Fu, G.: Comparative Analysis of ImageNet Pre-Trained Deep Learning Models and DINOv2 in Medical Imaging Classification. arXiv. arXiv:2402.07595 (2024)

[17] Isensee, F., Jaeger, P.F., Kohl, S.A.A. et al.: nnU-Net: a self-configuring method for deep learning-based biomedical image segmentation. Nat Methods 18, 203–211. https://doi.org/10.1038/s41592-020-01008-z (2021)

[18] Jiang, N., et al.: Vision transformers don't need trained registers. NeurIPS. arXiv:2506.08010 (2025)

[19] Khattak, M., Kunhimon,S., Naseer, M., Khan, S., Khan, F.: UniMed-CLIP: Towards a Unified Image-Text Pretraining Paradigm for Diverse Medical Imaging Modalities. arXiv. arXiv:2412.10372 (2024)

[20] Kirillov, A. et al.: SAM: Segment Anything. arXiv. arXiv:2304.02643 (2023)

[21] Koch, V., Wagner, S., Kazeminia, S., Sancar, E., Hehr, M., Schnabel, J., Peng, T., Marr, C.: DinoBloom: A Foundation Model for Generalizable Cell Embeddings in Hematology. arXiv. arXiv:2404.05022 (2024)

[22] Kovalyk, O. et al.: PAPILA: dataset with fundus images and clinical data of both eyes of the same patient for glaucoma assessment. Sci. Data 9, 291 (2022).

[23] Lin, T., Goyal, P., Girshick, R., He, K., Dollar, P.: Focal loss for dense object detection. ICCV (2017)

[24] Loshchilov, I., Hutter, F.: Decoupled weight decay regularization. ICLR (2019)

[25] Ma, C., Tan, W., He, R. et al.: Pretraining a foundation model for generalizable fluorescence microscopy-based image restoration. Nat Methods 21, 1558–1567. https://doi.org/10.1038/s41592-024-02244-3 (2024)

[26] Mann, H. B., Whitney, D. R.: On a Test of Whether one of Two Random Variables is Stochastically Larger than the Other. The Annals of Mathematical Statistics, 18(1), 50–60. http://www.jstor.org/stable/2236101 (1947)

[27] Martin, D., Fowlkes, C., Tal, D., Malik, J.: A Database of Human Segmented Natural Images and its Application to Evaluating Segmentation Algorithms and Measuring Ecological Statistics. ICCV (2001).

[28] Martinsson, P.-G. and Tropp, J.A.: 'Randomised embeddings', in Randomized Numerical Linear Algebra: Foundations & Algorithms. arXiv preprint arXiv:2002.01387 (2020)

[29] Milletari, F. Navab, N., Ahmadi, S.: V-Net: Fully convolutional neural networks for volumetric medical image segmentation. 3DV, (2016)

[30] Oquab, M., Darcet, T., Moutakanni, T., Vo, H., Szafraniec, M., Khalidov, V., Fernandez, P., Haziza, D., Massa, F., El-Nouby, A., et al.: Dinov2: Learning robust visual features without supervision. arXiv preprint arXiv:2304.07193 (2023)

[31] Porwal, P. et al.: IDRiD: diabetic retinopathy - segmentation and grading challenge. Med. Image Anal. 59, 101561 (2020)

[32] Radford et al.: CLIP: Learning Transferable Visual Models From Natural Language Supervision. ICML. arXiv:2103.00020 (2021)

[33] Ronneberger, O., Fischer, P., Brox, T.: U-Net: Convolutional Networks for Biomedical Image Segmentation. arXiv. arXiv:1505.04597 (2015)

[34] Russakovsky, O., Deng, J., Su, H., Krause, J., Satheesh, S., Ma, S., Huang, Z., Karpathy, A., Khosla A., Bernstein, M., Berg, A. C., and Fei-Fei, L.: Imagenet large scale visual recognition challenge. IJCV. arXiv:1409.0575 (2015)

[35] Sablayrolles A., Douze M., Schmid C., and Jégou H.: Spreading vectors for similarity search. ICLR (2019)

[36] Silberman, N., Hoiem, D., Kohli, P., Fergus, R.: Indoor segmentation and support inference from rgbd images. ECCV (2012)

[37] Siméoni, O., et al.: Localizing objects with self-supervised transformers and no labels. BMVC. arXiv:2109.14279. (2021)

[38] Sun, M., et al.: Massive activations in large language models. COLM. arXiv:2402.17762 (2024)

[39] Vaswani, A., Shazeer, N., Parmar, N., Uszkoreit, J., Jones, L., Gomez, A., Kaiser, L., Polosukhin, I.: Attention is all you need. arXiv preprint arXiv:1706.03762 (2017)

[40] Wang, H., Zhang, T., Salzmann, M.: SINDER: Repairing the Singular Defects of DINOv2. ECCV. arXiv:2407.16826 (2024)

[41] Xiao, G., et al.: Efficient streaming language models with attention sinks. ICLR. arXiv:2309.17453 (2024)

[42] Yang, J., et al.: Denoising Vision Transformers. ECCV. arXiv:2401.02957 (2024)

[43] Zhou, Y., Chia, M.A., Wagner, S.K. et al.: A foundation model for generalizable disease detection from retinal images. Nature 622, 156–163 https://doi.org/10.1038/s41586-023-06555-x (2023)

[44] Zhou, J., Wei, C., Wang, H., Shen, W., Xie, C., Yuille, A., and Kong, T.: ibot: Image bert pre-training with online tokenizer. ICLR (2022)

[45] Zhou, B., Zhao, H., Puig, X., Fidler, S., Barriuso, A., and Torralba, A.: Scene parsing through ade20k dataset. CVPR (2017)

[46] Zu, W., Xie, S., Chen, H., Ma, L.: Pre-trained Models Succeed in Medical Imaging with Representation Similarity Degradation. arXiv. arXiv:2503.07958 (2025)

A Technical Appendices and Supplementary Material

A.1 Supplementary Figures

Figure 5 shows fine-tuning with RMLPs create tokens with smaller norm and that it assigns bigger norms to patch tokens coming from high-information regions unlike when fine-tuning with MLPs.

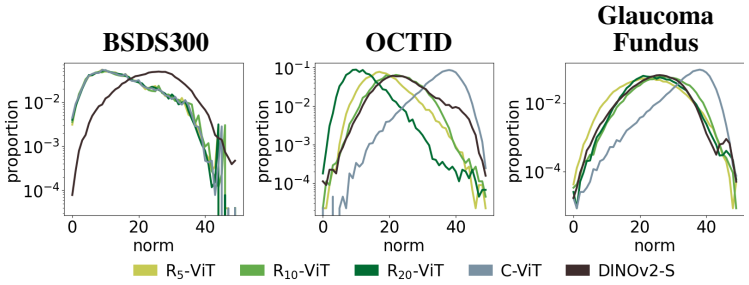

(a) Proportion curves of attention maps' norms.

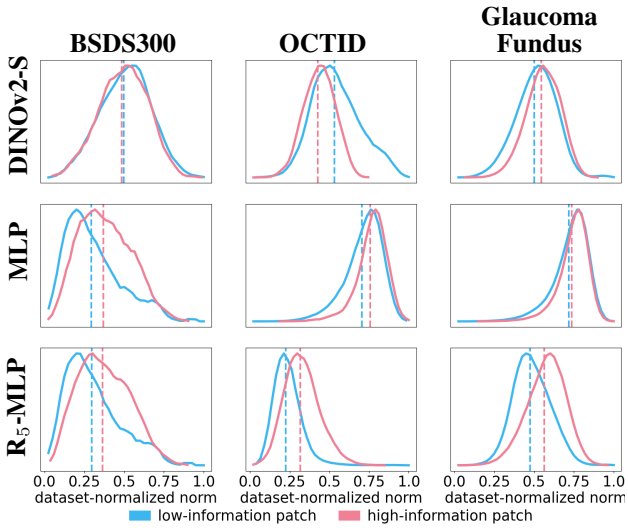

(b) Normalized probability density functions of attention maps' norms for low- and high-information patches across models (rows) and datasets (columns). Low- and high-content patches are classified by a two-component Gaussian Mixture model fitted on smoothed pixel gradients averaged per patch. Dashed lines stand for expected value.

Figure 5: Visualization of second- (BSDS300 [27]) and first-order (OCTID [14]/Glaucoma Fundus [2]) attention maps' norm statistics. **Subfigure (a):** Proportion curves. **Subfigure (b):** Normalized probability density functions for low- and high-information patches.

The following visualizations for the first- and second-order attention maps as well as the PCA visualizations were computed following a sliding window approach.

Here we present some extra examples on the performance of DINOv2-S, DINOv2-S+MLP and DINOv2-S+R_λ-MLP in natural, OCT and CFP modalities, in addition of RETFound [43] for the ophthalmology modalities mentioned before.

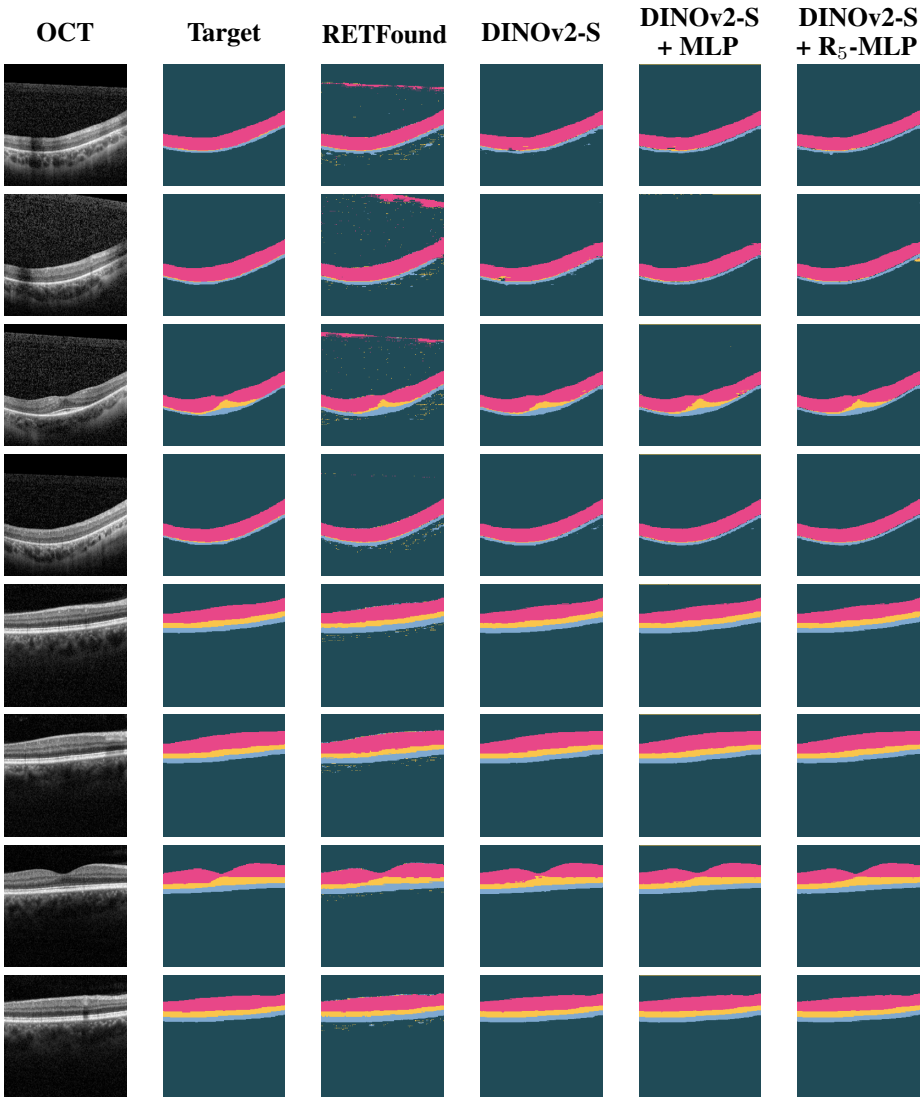

Figure 6: OCT segmentation on the dataset from Eckardt, et al. [12] using different backbones (columns) in a ViT-UNet hybrid

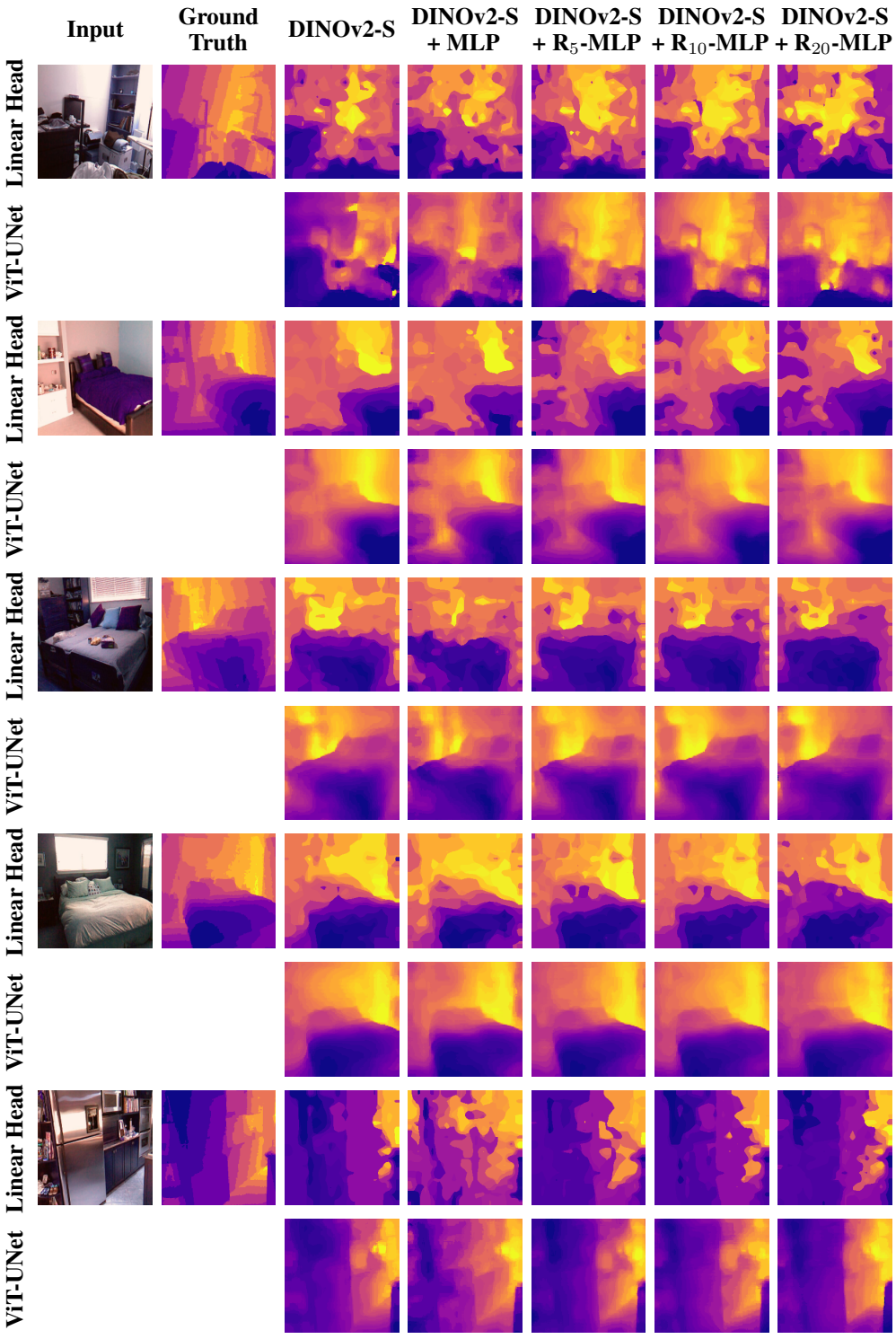

Figure 7: Depth estimation of NYU-Depth V2 [36] dataset using various backbones (last five columns) with a linear head or ViT-UNet hybrid.

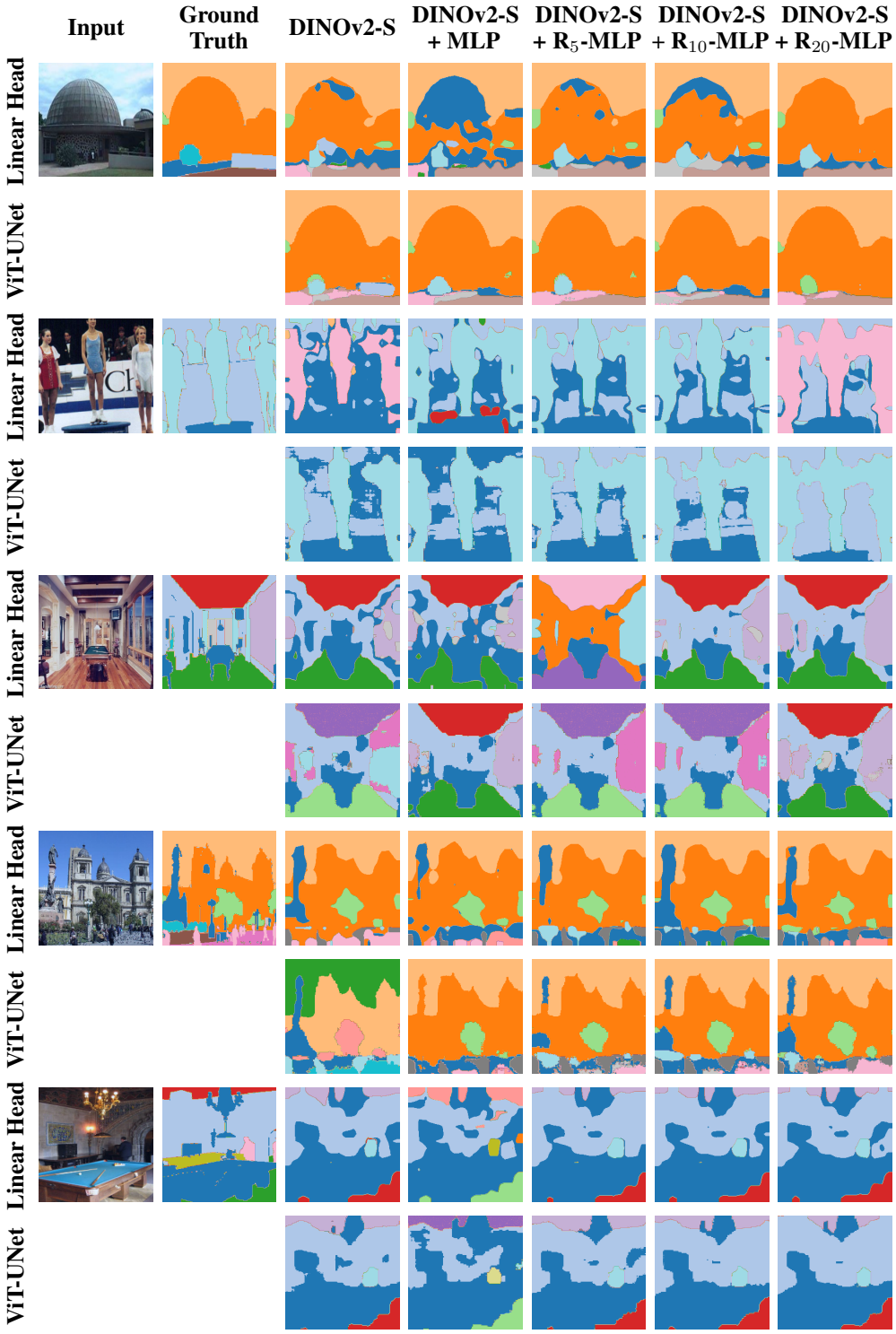

Figure 8: Semantic segmentation of ADE20k [45] dataset using various backbones (last five columns) with a linear head or ViT-UNet hybrid.

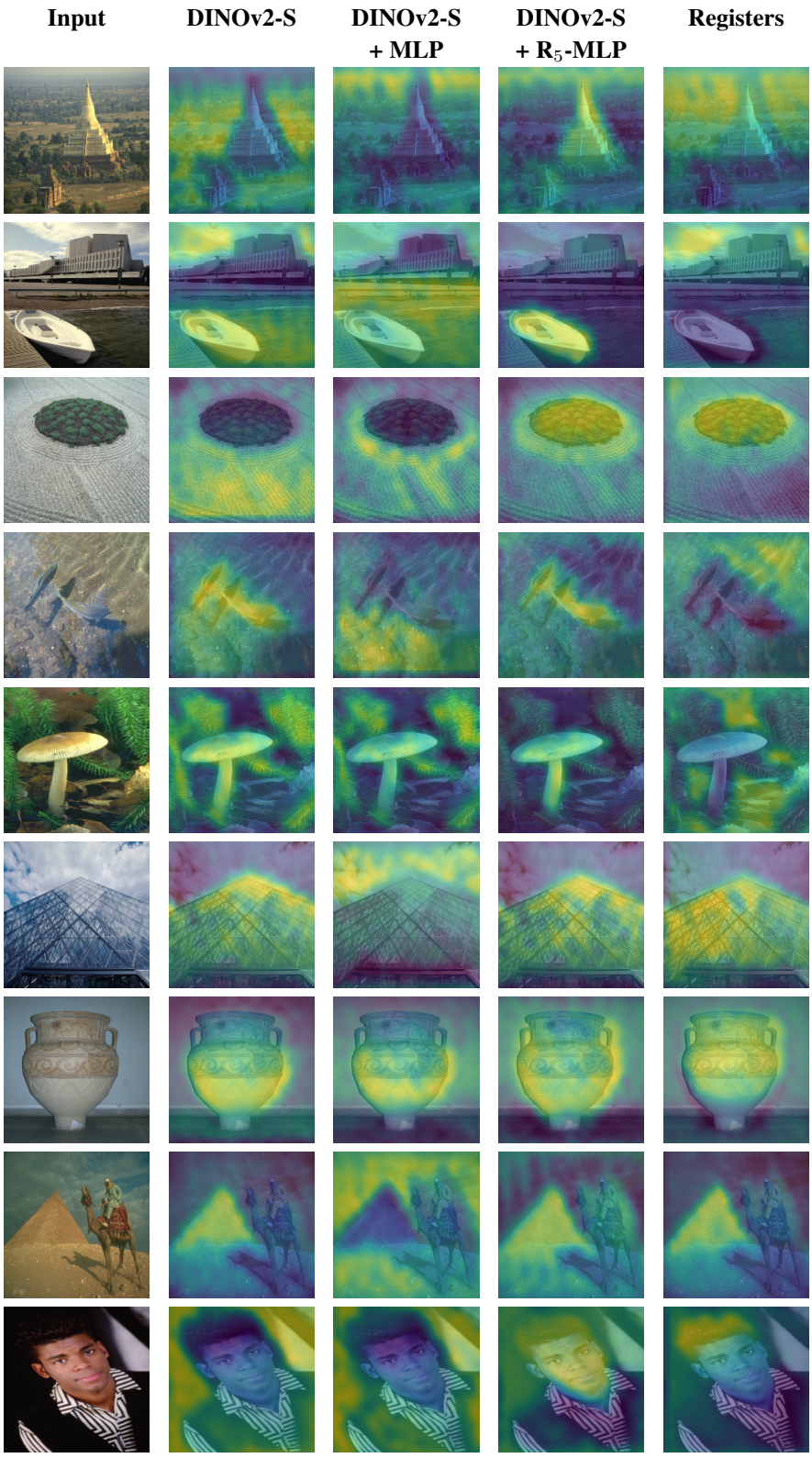

Figure 9: Second-order attention maps on the BSDS300 [27] dataset. Patch tokens were extracted using different backbones (columns).

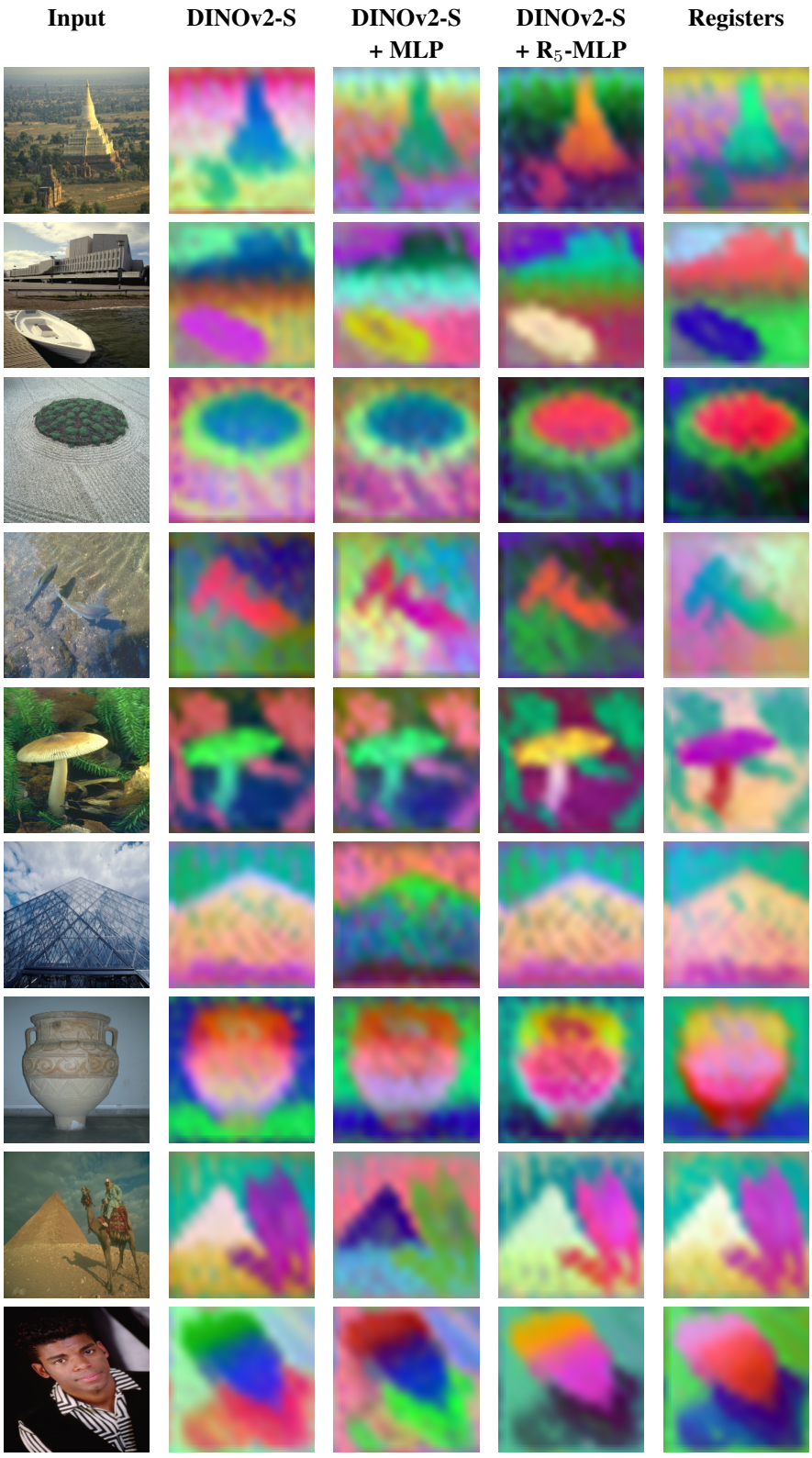

Figure 10: PCA visualization of embedding of BSDS300 [27] dataset using different backbones (columns).

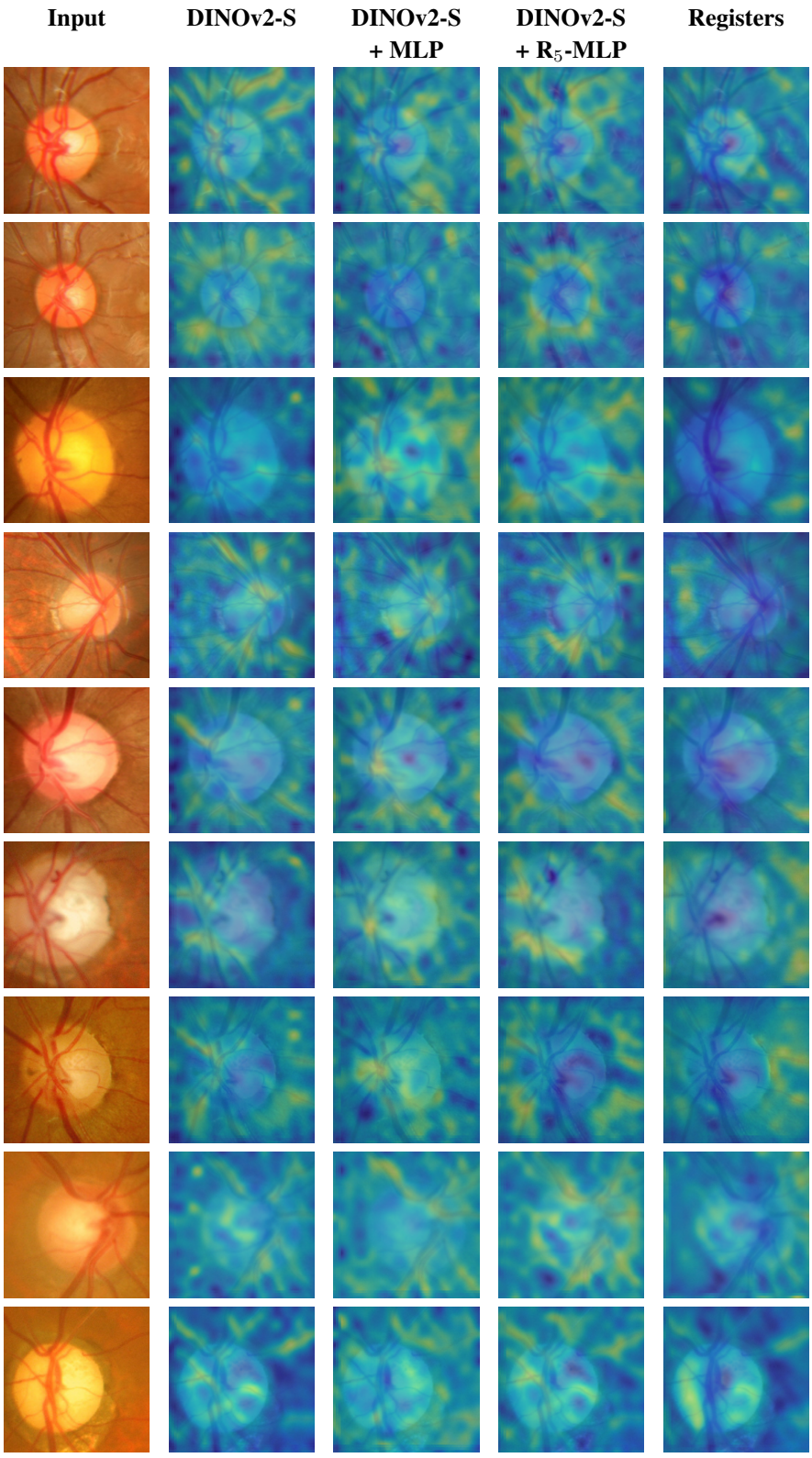

Figure 11: First-order attention maps on Glaucoma Fundus [2] dataset using different backbones (columns).

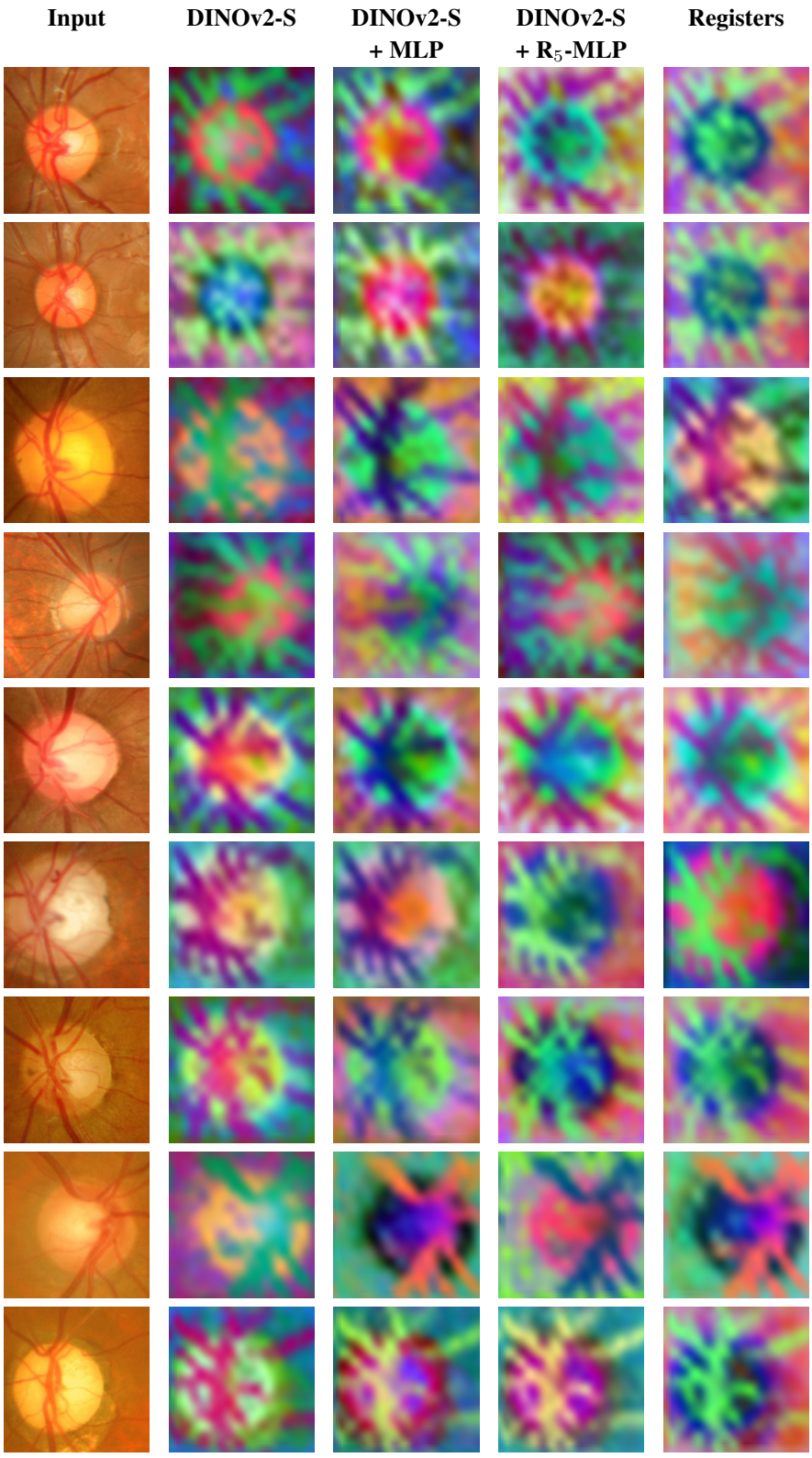

Figure 12: PCA visualization of embeddings of Glaucoma Fundus [2] dataset using different backbones (columns).

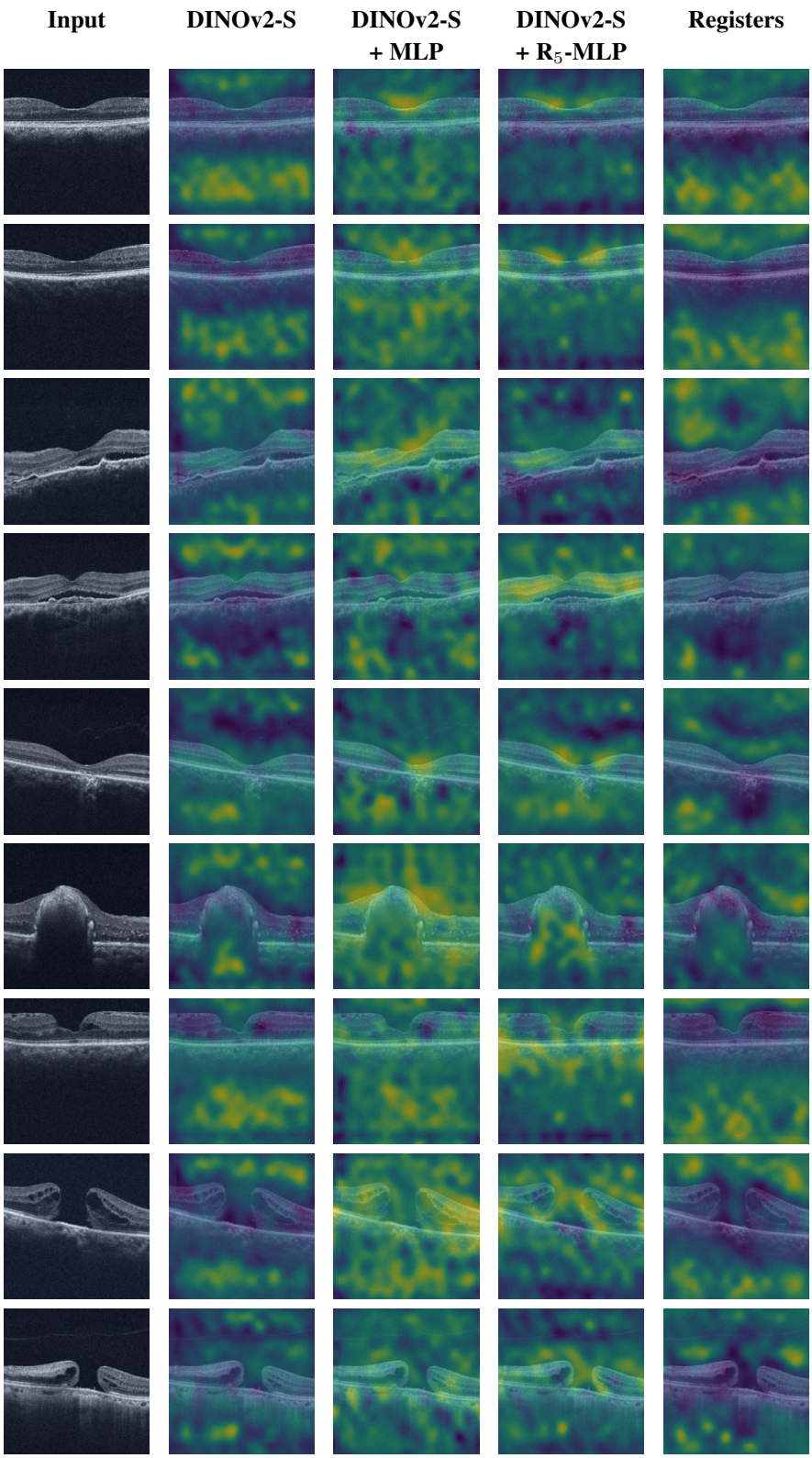

Figure 13: First-order attention maps on OCTID [14] dataset using different backbones (columns).

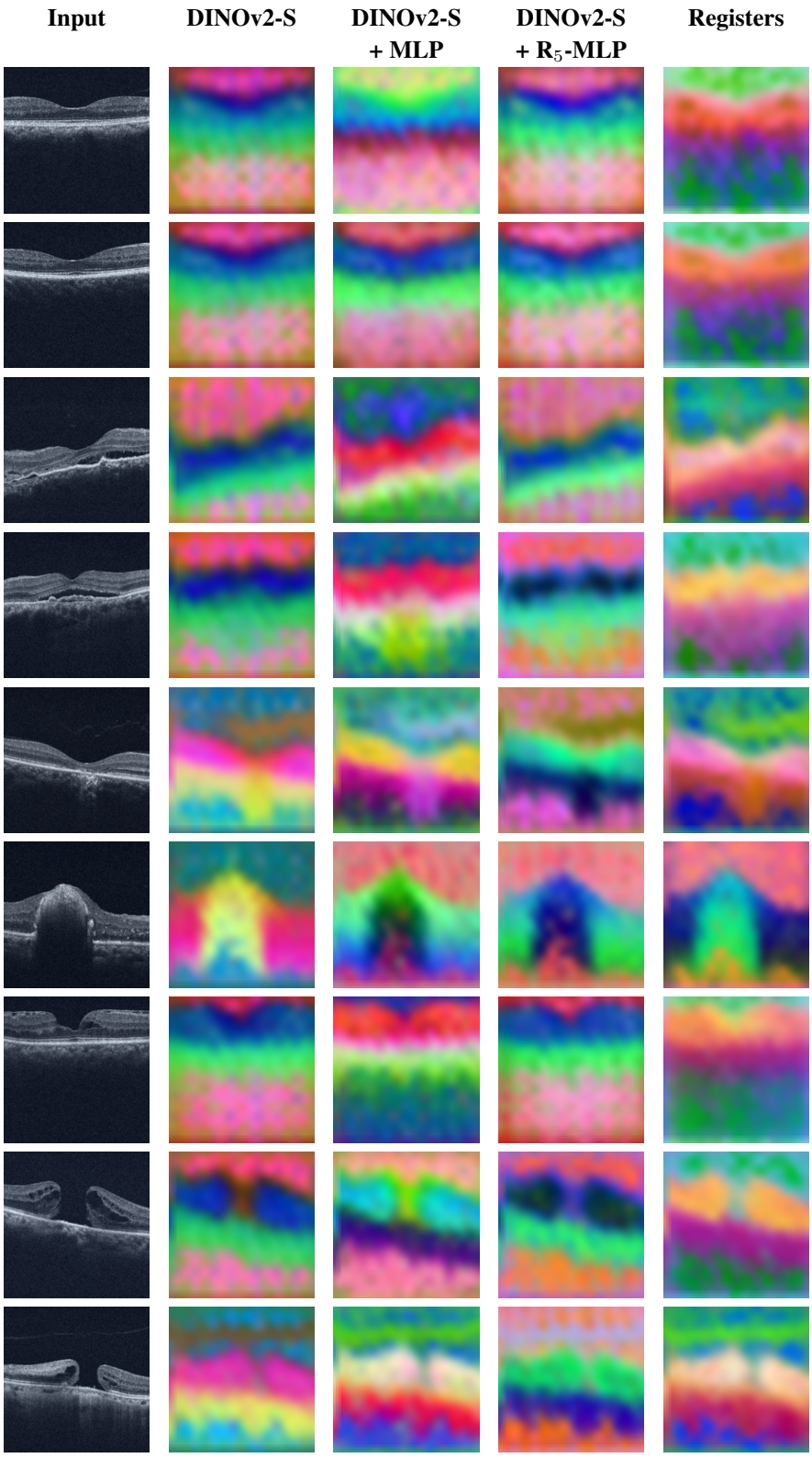

Figure 14: PCA visualization of embeddings of OCTID [14] dataset using different backbones (columns).

A.2 Mathematical Definitions and Proofs

Given the interdisciplinary of the theoretical analysis in this paper, not only across scientific fields, but also across mathematical domains, we first provide a list of useful mathematical definitions results to analytically understand the results in this paper.

A.2.1 General Mathematical Background

We present now a collection of topological definitions and a result.

Definition 6. *Given a function $f : X \to Y$, we will say that f is locally injective on a subset $A \subseteq X$ if, $\forall x \in A$, $\exists U_x \subseteq X$ open such that $f|_{U_x}$ is injective.*

Definition 7. *Given a metric space (X, δ), a subset $A \subseteq X$ and $\varepsilon > 0$, we call a ε-cloud to the set $\{x \in X : \delta(x, A) < \varepsilon\}$.*

Definition 8. *Given a topological space X, we will say X is disconnected if there are $A, B \subseteq X$ such that they are open and non-empty, $A \cap B = \varnothing$ and $A \cup B = X$. In addition, we will call $\{A, B\}$ a disconnection.*

Definition 9. *Given a topological space X and $D \subseteq X$, we will say D is dense in X is for whatever open subset $U \subseteq X$, $U \cap D \neq \varnothing$*

Remark 10. *If $f : X \to Y$ is continuous and Y is disconnected, X is disconnected.*

Proof. Let $\{A, B\}$ be a disconnection for Y. Then $f^{-1}[A]$ and $f^{-1}[B]$ are open and non-empty due to f being continuous and a function resp. Furthermore, $f^{-1}[A] \cup f^{-1}[B] = X$ since f is a function and $\{A, B\}$ a disconnection. Lastly, using that $\{A, B\}$ is a disconnection and knowing that the pre-image opens finite intersections, $f^{-1}[A] \cap f^{-1}[B] = f^{-1}[A \cap B] = f^{-1}[\varnothing] = \varnothing$. □

A.2.2 Topological Analysis of Vision Transformers

In this subsection, we will present a mathematical model describing ViTs and proving some results on their topological properties. Notably, the only assumption we are making in this subsection is that the corresponding ViT was trained using the KoLeo [35] regularizer.

Theorem 11. *ViTs can be decomposed as a tokenization function followed by a composition of translations. Said translations are defined by local orthonormal bases generated by the modulation of the data via the queries, keys and values layers.*

Proof. Let Ω be an image domain and $\Psi := \bigcup_{n \in \mathbb{N}} \mathbb{R}^{n \times d}$ be the ViT's latent space and d its token dimension. Further, let $\mathcal{V} : \Omega \to \Psi$ denote the ViT as a learnable function and $T : \Psi \to \Psi$ the transformer encoder, following the structure from Dosovitskiy et al. [11]. We decompose these maps as $\mathcal{V} = T \circ \mathcal{C}$ and $T = \mathcal{N} \circ T_{L-1} \circ ... \circ T_0$, respectively where $\mathcal{C}$ is a continuous map from Ω to Ψ, $\mathcal{N}$ is a normalization layer and for each $l \in \{0, \dots, L-1\}$, we define

$$\begin{aligned} T_l : \Psi &\to \Psi \\ x &\mapsto x + s_l(x) \end{aligned}$$

with $s_l : \Psi \to \Psi$ described below.

Leaving the normalization $\mathcal{N}$ aside, we can see T as a translation defined as a composition of the residual steps s_l. Following Vaswani et al. [39], s_l can be further decomposed as

$$s_l : x \mapsto f_l\left(\mathcal{N}_{2,l}(x + h_l(\mathcal{N}_{1,l}(x)))\right)$$

where h_l represents the multi-head self-attention mechanism, f_l is the MLP block and $\mathcal{N}_{1,l}$ and $\mathcal{N}_{2,l}$ are layer normalizations.

Assuming linear layers have no bias for simplicity, the attention h_l can be expressed as

$$h_l : x \mapsto \sigma\left(\frac{1}{r}\mathcal{L}_{Q,l}(xx^T)\mathcal{L}_{K,l}^T\right)\mathcal{L}_{V,l}x$$

where σ is the softmax function, r is a scaling factor and $\mathcal{L}_{V,l}, \mathcal{L}_{K,l}, \mathcal{L}_{Q,l}$ are learnable linear maps for queries, keys, and values.

Since xx^T is symmetric, it can be diagonalized, allowing h_l to be rewritten as

$$h_l : x \mapsto \sigma\left(\frac{1}{r}\mathcal{L}'_{Q,l} D_x \mathcal{L}'_{K,l}\right)\mathcal{L}_{V,l} x$$

where D_x is diagonal and $\mathcal{L}'_Q$ and $\mathcal{L}'_K$ incorporate the change of basis.

Thus, we can understand T as a map creating a field for the embeddings to follow, where the self-attention layers dynamically generate local orthonormal bases over Ψ that the queries, keys and value matrices then modulate while the MLPs f_l refine the resulting directions. □

Lemma 12. *If a continuous function $f : X \to Y$ is locally injective on a compact set $K \subseteq X$ and the topology on X is induced by a metric δ, then $\exists \varepsilon > 0$ such that f is injective on*

$$\{x \in X : \delta(x, K) < \varepsilon\}.$$

Proof. Let $U_\varepsilon := \{x \in X : \delta(x, K) < \varepsilon\}$ and let us work by contradiction, i.e. we will assume $\forall \varepsilon > 0$, $\exists \{x_\varepsilon, y_\varepsilon\} \subseteq U_\varepsilon$ such that $x_\varepsilon \neq y_\varepsilon$ and $f(x_\varepsilon) = f(y_\varepsilon)$. Given this, we can construct two sequences such that for $n \in \mathbb{N}^+$, $\{x_n, y_n\} \subseteq U_{1/n}$, $x_n \neq y_n$ and $f(x_n) = f(y_n)$.

Since K is compact, it is easy to see that for every positive natural number $\overline{U_{1/n}}$ is compact too. Thus, given X is metric and $\{x_n\}_{n>0}, \{y_n\}_{n>0} \subseteq \overline{U_1}$, we can extract convergent subsequences $\{x_{n_i}\}_{i>0}, \{y_{n_i}\}_{i>0}$ to x and y respectively.

Let us notice that $K = \bigcap_{n>0} U_{1/n}$. Therefore $\{x, y\} \subseteq K \Rightarrow f(x) = f(y)$ since f is continuous and injective in K, having $x = y$ as a consequence. Also, since f is locally injective, $\exists V_x$ open such that $x \in V_x$ and f is injective on it and since $\{x_{n_i}\}_{i>0}, \{y_{n_i}\}_{i>0}$ both converge to x, $\exists N \in \mathbb{N}$ such that $\forall i > N, \{x_{n_i}, y_{n_i}\} \subset V_x \Rightarrow f(x_{n_i}) = f(y_{n_i})\, \forall i > N$, reaching this way the contradiction we were looking for.

□

Lemma 13. *If a function $f : X \to Y$ is injective and continuous with compact domain and Hausdorff codomain, f is an homeomorphism on $f[X]$.*

Proof. Assuming the hypothesis from the lemma, the only thing remaining to show is that f is open.

Thing being this way, let us take an open set $U \subseteq X$. Then $X \backslash U$ is closed which turns it into a compact set since X is compact. Thus, by continuity, $f[X \backslash U]$ is compact, which makes it closed since Y is Hausdorff, forcing $f[U]$ to be open.

□

A.2.3 RMLPs as Stochastic Regularizer for ViTs

We now introduce some useful definitions and rigorous proofs on the way RMLPs regularize the representation's topology by making the ViT perceive points in the representation space as ball of certain radius with high probability.

Definition 14. *[28] Let $E \subset \mathbb{F}^n$ a set and $\varepsilon \in (0, 1)$ be a distortion parameter. We say that a linear map $S : \mathbb{F}^n \to \mathbb{F}^m$ produces an ε-distortion of E if, $\forall x \in E$,*

$$(1 - \varepsilon)\|x\|_2 \leqslant \|Sx\|_2 \leqslant (1 + \varepsilon)\|x\|_2.$$

Remark 15. *If $x \in \mathbb{R}^d$ and Γ is a $n \times d$ matrix with iid entries and such that $\Gamma_{i,j} \sim \mathcal{N}(0, \sigma^2)$, then $\mathbb{E}[\|\Gamma x\|_2^2] = d\sigma^2 \|x\|_2^2$.*

Proof. Computing

$$\mathbb{E}[\|\Gamma x\|_2^2] = \mathbb{E}[\Sigma_i \left(\Sigma_j \Gamma_{ij} x_j\right)^2] = \Sigma_i \mathbb{E}[(\Sigma_j \Gamma_{ij} x_j)^2].$$

Since the entries of Γ are independent and $\Gamma_{i,j} \sim \mathcal{N}(0, \sigma^2)$, we then have

$$\mathbb{E}[\|\Gamma x\|_2^2] = \Sigma_i \Sigma_j x_j^2 \mathbb{E}[\Gamma_{jj}^2] = d\sigma^2 \|x\|_2^2.$$

□

Definition 16. *Let $S \in \mathbb{F}^{m \times n}$ be a linear map and $E \subseteq \mathbb{S}^{n-1}(\mathbb{F})$ a subset of the unit sphere in $\mathbb{F}^n$. Then, Martinsson and Tropp [28] define the minimum and maximum restricted singular values respectively as*

$$\sigma_{\min}(S, E) := \min_{x \in E} \|Sx\| \qquad \textit{and} \qquad \sigma_{\max}(S, E) := \max_{x \in E} \|Sx\|.$$

Lemma 17. *[28] Let us consider $\{a_1, \ldots, a_N\} \subseteq \mathbb{R}^d$, $\Gamma \in \mathbb{R}^{n \times d}$ and build*

$$E = \left\{ \frac{a_i - a_j}{||a_i - a_j||} : 1 \leqslant i < j \leqslant N \right\} \subseteq \mathbb{S}^{d-1}.$$

Then we have the following probability bounds:

$$\mathbb{P}\left\{ \sigma_{\min}(\Gamma, E) \leqslant 1 - \frac{1 + 2\sqrt{\log(N/2)}}{\sqrt{n}} - t \right\} \leqslant e^{-dt^2/2}$$

and

$$\mathbb{P}\left\{ \sigma_{\max}(\Gamma, E) \geqslant 1 + \frac{2\sqrt{\log(N/2)}}{\sqrt{d}} + 1 \right\} \leqslant e^{-dt^2/2}.$$

Thus, it is sufficient that $n \geqslant 8\varepsilon^{-2} \log N$ for being able to guarantee Γ has a distortion of ε 14 with high probability.

Corollary 18. *If $\mathcal{A} \subseteq \Omega$ is the training data, and T is locally injective on $\mathcal{A}$, the following holds:*

- *) There exists $\varepsilon > 0$ such that T is an homeomorphism on an ε-cloud containing $\mathcal{A}$ (see Def. 7).*
- ·) *Let $P, Q \subseteq \Omega$. $\mathcal{C}[P] \cup \mathcal{C}[Q]$ is disconnected in Ψ if and only if $\mathcal{V}[P] \cup \mathcal{V}[Q]$ is disconnected in Ψ (see Def. 8), which can contribute to the batch effect.*
- :) *If $D \subseteq \Psi$ is dense in Ψ (see Def. 9), then $\mathcal{V}[D]$ is dense in $\mathcal{V}[\Psi]$.*

Proof. Assuming the corollary hypothesis, let us prove the statements.

) The existence of the ε-cloud is direct result of theorem 2.

·) The result follows directly from Theorem 2 since homeomorphisms preserve connections and disconnections.

:) Let D be dense in Ψ. We note $\mathcal{C}$ is continuous for being defined as a multiplication of matrices and addition of vectors. Thus $\mathcal{C}[D]$ is dense in $\mathcal{C}[\Omega]$. Therefore, $\mathcal{V}[D]$ is dense in $\mathcal{V}[\Omega]$ since T is an homeomorphism because of theorem 2.

□

Theorem 19. *Being $\{p_1, \ldots, p_N\} \subseteq R^m$, $\varepsilon > 0$, $\lambda > 0$ and Γ a matrix of size $n \times m$ whose entries are iid and following a normal distribution $\mathcal{N}(0, \lambda n^{-1})$, Γ will have an ε distortion on the set*

$$E := \left\{ \frac{p_i - p_j}{\|p_i - p_j\|} : 1 \leqslant i < j \leqslant N \right\}$$

with high probability if

$$\lambda n^{-1} < \frac{\varepsilon^2}{8 \ln N}.$$

In addition,

$$\mathbb{E}[\|\Gamma x\|_2^2] = m\lambda n^{-1}\|x\|_2^2.$$

Proof. To see $\mathbb{E}[\|\Gamma x\|_2^2] = m\lambda n^{-1}\|x\|_2^2$, it is enough to use remark 15.

On the other hand, to compute the distortion of Γ, let us assume the hypothesis and define the restricted singular values following Martinsson and Tropp [28] as

$$\sigma_{\min}(\Gamma, E) := \min_{x \in E} \|\Gamma x\| \qquad \sigma_{\max}(\Gamma, E) := \max_{x \in E} \|\Gamma x\|,$$

let us realize the statement is equivalent to having

$$1 - \varepsilon < \sigma_{\min}(\Gamma, E) \leqslant \|\Gamma x\| \leqslant \sigma_{max}(\Gamma, E) < 1 + \varepsilon.$$

Thus, having $\sqrt{\lambda/d} < \varepsilon/\sqrt{8 \ln N}$, it follows $\varepsilon > \sqrt{\lambda/n}\left(1 + 2\sqrt{\ln(N/2)}\right)$ and then $1 - \varepsilon < 1 - \sqrt{\lambda/n}\left(1 + 2\sqrt{\ln(N/2)}\right)$. This way, we can take $t > 0$ and write

$$\mathbb{P}\left(\sigma_{\min}(\Gamma, E) \leqslant 1 - \varepsilon - t\right) \leqslant \mathbb{P}\left(\sigma_{\min}(\Gamma, E) \leqslant 1 - \sqrt{\lambda/n}\left(1 + 2\sqrt{\ln(N/2)}\right) - t\right).$$

Similarly, $\sqrt{\lambda/n} < \varepsilon/\sqrt{8 \ln N}$ implies $1 + \varepsilon > 1 + 2\sqrt{\lambda n^{-1} \ln(N/2)}$. Thus, being $t > 0$,

$$\mathbb{P}\left(\sigma_{\max}(\Gamma, E) \geqslant 1 + \varepsilon + t\right) \leqslant \mathbb{P}\left(\sigma_{\max}(\Gamma, E) \geqslant 1 + 2\sqrt{\lambda n^{-1} \ln(N/2)} + t\right).$$

Therefore, using that the Gaussian width of E, $w(E)$, satisfies $w(E) < 2\ln(N/2)$ and the theorem for restricted singular values and a Gaussian matrix from Martinsson and Tropp [28], for every $t > 0$ we have

$$\mathbb{P}\left(\sigma_{\min}(\Gamma, E) \leqslant 1 - \varepsilon - t\right) \leqslant e^{-\lambda^{-1} n t^2/2}$$

and

$$\mathbb{P}\left(\sigma_{\max}(\Gamma, E) \geqslant 1 + \varepsilon + t\right) \leqslant e^{-\lambda^{-1} n t^2/2}.$$

$\therefore$ Γ has an ε-distortion with high probability. □

A.3 Technical Details

Backbone Training. All training was performed on a single GPU (Quadro RTX153 8000 or NVIDIA A100-SXM4-40GB) and required approximately 15 hours per trained backbone, reflecting the low computational cost of our approach and its reduced environmental footprint. Models were trained on randomly sampled mini-batches until validation performance plateaued. For datasets without predefined splits, we manually partitioned them into 70% training, 15% validation, and 15% testing.

All models were trained using the AdamW optimizer [24], which we employed consistently across fine-tuning stages as well as during training of downstream linear heads and UNet decoders.

Table 5 shows the main hyperparameters used when fine-tuning DINOv2-S on natural, OCT and CFP modalities. Further implementation details can be found in our code.

Downstream Tasks Training. For classification tasks using DINOv2, we constructed the input representations for 1-Nearest Neighbor, Random Forest, and linear probing classifiers by concatenating the class token with the mean of the patch tokens. In contrast, for SwAV, which does not produce patch tokens, we used its output directly. The linear classifier was trained using the cross-entropy loss.

Table 5: Hyperparameters used for fine-tuning DINOv2-S to obtain C-ViT and R_λ-ViT.

Hyperparameter	Value
Optimizer	AdamW[24]
Plateau size for early stop	10 epochs
Batch size	32
Token's dimension	384
DINO coefficient	1
iBOT coefficient	1
KoLeo coefficient	0.5
Initial learning rate	1e-7
Patience/factor for learning rate scheduler	3/0.4
Minimum learning rate	1e-8
Hidden/Bottleneck/Output dimensions for MLPs and RMLPs	1536/256/65536
Number of transformer blocks	12
Patch size	14
Crop size	224
Steps per epoch	100
Warm up epochs	10

To integrate the ViT and UNet architectures for dense prediction tasks, we first projected the output of the ViT through a linear layer and then concatenated it with the features from the encoder branch of the UNet. This combined representation was subsequently fed into the UNet's decoder branch. The ViT outputs were handled differently depending on the task: for segmentation, we concatenated the class token with the patch tokens, while for depth estimation, only the patch tokens were used. Segmentation heads were trained using a weighted combination of focal loss and Dice loss, whereas depth estimation heads were trained using focal loss.

Evaluation of Patch Token Quality. First-order attention maps were computed by evaluating the norm of the patch token embeddings. For the second-order attention maps, we independently performed principal component analysis on the patch tokens of each image and calculated the norm of the top three principal components. To distinguish between low- and high-information patches within an image, we first computed the image gradient, applied a smoothing operation, and then averaged the resulting gradient values within each patch. A Gaussian Mixture Model with two components was subsequently used to classify the patches based on their average gradient magnitudes.

A.4 Information on External Sources

We used two pre-trained models in this work. Their licenses and repositories can be found in Table 6. A recollection of all the datasets used in this work can be found in Table 7a, both for natural and medical domains. To show the geographic diversity from our geographical dataset, we show the country of origin of the medical datasets used in this paper in Table 7b.

Table 6: External code and weights used as baselines.

Name	License	Repository
DINOv2 [30]	Apache-2.0	`https://github.com/facebookresearch/dinov2`
RETFound [43]	CC BY-NC 4.0	`https://github.com/rmaphoh/RETFound_MAE`
DVT [42]	MIT License	`https://github.com/Jiawei-Yang/Denoising-ViT`
Registers [9]	Apache-2.0	`https://github.com/facebookresearch/dinov2`
SwAV [4]	License: CC BY-NC 4.0	`https://github.com/facebookresearch/swav`
Sinder [40]	-	`https://github.com/haoqiwang/sinder`

Table 7: Used datasets, licenses and country of origin.

(a) Used datasets and their licenses.

Name	License	Repository
ImageNet-1k [34]	CC0: Public Domain	ImageNet-1k
NYU-Depth V2 [36]	MIT	NYU-Depth V2
ADE20k [45]	BSD-3-Clause	ADE20k
BSDS300 [27]	Non-commercial research	BDSD300
VOC07 [13]	Custom	PASCAL VOC 2007
OCTID [14]	CC0 1.0	OCTID
Glaucoma Fundus [2]	CC0 1.0	Glaucoma Fundus
IDRID [31]	Open Access	IDRID
JSIEC [7]	Open Access	JSIEC
MESSIDOR-2 [1, 10]	Non-commercial research	MESSIDOR-2
PAPILA [22]	GPL 3.0+	PAPILA
Retina [6]	Open Access	Retina
Aptos [3]	Custom	Aptos
Eckardt, et al. [12]	Property of LMU University Hospital	-

(b) Country of creation for medical dataset.

Dataset	Country
OCTID [14]	India
Glaucoma Fundus [2]	South Korea
IDRID [31]	India
JSIEC [7]	China
MESSIDOR-2 [1, 10]	France
PAPILA [22]	Spain
Retina [6]	Unspecified
Eckardt, et al. [12]	Germany

A.5 Supplementary Results

Table 8: DICE scores for segmentation on the Eckardt, et al. [12] dataset with emphasis on the Outer Nuclear Layer (ONL).

	ViT-UNet hybrid		Linear Head	
Model	Averaged DICE	DICE on ONL	Averaged DICE	DICE on ONL
RETFound [43]	0.92±0.06	0.59±0.10	0.10±0.02	0.01±0.02
DINOv2-S [30]	0.79±0.20	0.54±0.20	†0.16±0.08	**0.12±0.05*****
DINOv2-S+MLP	0.86±0.20	0.55±0.20	**0.20±0.05**	0.03±0.03
DINOv2-S+$R_{0.1}$-MLP	†0.94±0.12	†0.68±0.21	**0.20±0.03**	0.06±0.04
DINOv2-S+R_{5}-MLP	**0.97±0.03***	**0.72±0.09***	0.13±0.01	†0.08±0.03**
DINOv2-S+R_{10}-MLP	0.87±0.20	0.61±0.20	**0.20±0.01**	0.07±0.05*
DINOv2-S+R_{20}-MLP	0.70±0.30	0.47±0.20	0.13±0.02	0.07±0.05*
Eckardt, et al. [12]	0.92±0.03	0.44±0.03	–	–

NeurIPS Paper Checklist

1. **Claims**

   Question: Do the main claims made in the abstract and introduction accurately reflect the paper's contributions and scope?

   Answer: [Yes]

   Justification: In the abstract, we claim we developed a theoretical grounded regularizer that improves DINOv2-small's interpretability, mantains performance when fine-tuning on natural images and improves performance when trained in medical data. Data backing up this claims can be found in Figure 5 and Tables 1–3, respectively. In addition, it is discussed in Section 8.

   Guidelines:

   - The answer NA means that the abstract and introduction do not include the claims made in the paper.
   - The abstract and/or introduction should clearly state the claims made, including the contributions made in the paper and important assumptions and limitations. A No or NA answer to this question will not be perceived well by the reviewers.
   - The claims made should match theoretical and experimental results, and reflect how much the results can be expected to generalize to other settings.
   - It is fine to include aspirational goals as motivation as long as it is clear that these goals are not attained by the paper.

2. **Limitations**

   Question: Does the paper discuss the limitations of the work performed by the authors?

   Answer: [Yes]

   Justification: We discuss the limitations of the paper in Section 7 on a specific subsection.

   Guidelines:

   - The answer NA means that the paper has no limitation while the answer No means that the paper has limitations, but those are not discussed in the paper.
   - The authors are encouraged to create a separate "Limitations" section in their paper.
   - The paper should point out any strong assumptions and how robust the results are to violations of these assumptions (e.g., independence assumptions, noiseless settings, model well-specification, asymptotic approximations only holding locally). The authors should reflect on how these assumptions might be violated in practice and what the implications would be.
   - The authors should reflect on the scope of the claims made, e.g., if the approach was only tested on a few datasets or with a few runs. In general, empirical results often depend on implicit assumptions, which should be articulated.
   - The authors should reflect on the factors that influence the performance of the approach. For example, a facial recognition algorithm may perform poorly when image resolution is low or images are taken in low lighting. Or a speech-to-text system might not be used reliably to provide closed captions for online lectures because it fails to handle technical jargon.
   - The authors should discuss the computational efficiency of the proposed algorithms and how they scale with dataset size.
   - If applicable, the authors should discuss possible limitations of their approach to address problems of privacy and fairness.
   - While the authors might fear that complete honesty about limitations might be used by reviewers as grounds for rejection, a worse outcome might be that reviewers discover limitations that aren't acknowledged in the paper. The authors should use their best judgment and recognize that individual actions in favor of transparency play an important role in developing norms that preserve the integrity of the community. Reviewers will be specifically instructed to not penalize honesty concerning limitations.

3. **Theory assumptions and proofs**

Question: For each theoretical result, does the paper provide the full set of assumptions and a complete (and correct) proof?

Answer: [Yes]

Justification: All our theorems are properly proved in the main paper (Section 4) or in Appendix A.2). Same for needed mathematical definitions and related results.

Guidelines:

- The answer NA means that the paper does not include theoretical results.
- All the theorems, formulas, and proofs in the paper should be numbered and cross-referenced.
- All assumptions should be clearly stated or referenced in the statement of any theorems.
- The proofs can either appear in the main paper or the supplemental material, but if they appear in the supplemental material, the authors are encouraged to provide a short proof sketch to provide intuition.
- Inversely, any informal proof provided in the core of the paper should be complemented by formal proofs provided in appendix or supplemental material.
- Theorems and Lemmas that the proof relies upon should be properly referenced.

4. **Experimental result reproducibility**

Question: Does the paper fully disclose all the information needed to reproduce the main experimental results of the paper to the extent that it affects the main claims and/or conclusions of the paper (regardless of whether the code and data are provided or not)?

Answer: [Yes]

Justification: We describe in detail the regularization method in Section 3, specifying that the training algorithm is the same as the one from DINOv2 [30].

Guidelines:

- The answer NA means that the paper does not include experiments.
- If the paper includes experiments, a No answer to this question will not be perceived well by the reviewers: Making the paper reproducible is important, regardless of whether the code and data are provided or not.
- If the contribution is a dataset and/or model, the authors should describe the steps taken to make their results reproducible or verifiable.
- Depending on the contribution, reproducibility can be accomplished in various ways. For example, if the contribution is a novel architecture, describing the architecture fully might suffice, or if the contribution is a specific model and empirical evaluation, it may be necessary to either make it possible for others to replicate the model with the same dataset, or provide access to the model. In general. releasing code and data is often one good way to accomplish this, but reproducibility can also be provided via detailed instructions for how to replicate the results, access to a hosted model (e.g., in the case of a large language model), releasing of a model checkpoint, or other means that are appropriate to the research performed.
- While NeurIPS does not require releasing code, the conference does require all submissions to provide some reasonable avenue for reproducibility, which may depend on the nature of the contribution. For example
  (a) If the contribution is primarily a new algorithm, the paper should make it clear how to reproduce that algorithm.
  (b) If the contribution is primarily a new model architecture, the paper should describe the architecture clearly and fully.
  (c) If the contribution is a new model (e.g., a large language model), then there should either be a way to access this model for reproducing the results or a way to reproduce the model (e.g., with an open-source dataset or instructions for how to construct the dataset).
  (d) We recognize that reproducibility may be tricky in some cases, in which case authors are welcome to describe the particular way they provide for reproducibility. In the case of closed-source models, it may be that access to the model is limited in some way (e.g., to registered users), but it should be possible for other researchers to have some path to reproducing or verifying the results.

5. **Open access to data and code**

   Question: Does the paper provide open access to the data and code, with sufficient instructions to faithfully reproduce the main experimental results, as described in supplemental material?

   Answer: [Yes]

   Justification: The models presented in this paper were trained on public datasets, with the exception of the dataset presented by Eckardt, et al. [12]. This dataset was used to trained the OCT segmentation task, but cannot be released due to data privacy laws. Regarding code, well-documented code for reproducing our experiments will be released after acceptance to preserve anonymity. Same for the trained weights of the models presented here.

   Guidelines:

   - The answer NA means that paper does not include experiments requiring code.
   - Please see the NeurIPS code and data submission guidelines (`https://nips.cc/public/guides/CodeSubmissionPolicy`) for more details.
   - While we encourage the release of code and data, we understand that this might not be possible, so "No" is an acceptable answer. Papers cannot be rejected simply for not including code, unless this is central to the contribution (e.g., for a new open-source benchmark).
   - The instructions should contain the exact command and environment needed to run to reproduce the results. See the NeurIPS code and data submission guidelines (`https://nips.cc/public/guides/CodeSubmissionPolicy`) for more details.
   - The authors should provide instructions on data access and preparation, including how to access the raw data, preprocessed data, intermediate data, and generated data, etc.
   - The authors should provide scripts to reproduce all experimental results for the new proposed method and baselines. If only a subset of experiments are reproducible, they should state which ones are omitted from the script and why.
   - At submission time, to preserve anonymity, the authors should release anonymized versions (if applicable).
   - Providing as much information as possible in supplemental material (appended to the paper) is recommended, but including URLs to data and code is permitted.

6. **Experimental setting/details**

   Question: Does the paper specify all the training and test details (e.g., data splits, hyperparameters, how they were chosen, type of optimizer, etc.) necessary to understand the results?

   Answer: [Yes]

   Justification: Experimental settings are described in Section 5. Further, code will be released after acceptance.

   Guidelines:

   - The answer NA means that the paper does not include experiments.
   - The experimental setting should be presented in the core of the paper to a level of detail that is necessary to appreciate the results and make sense of them.
   - The full details can be provided either with the code, in appendix, or as supplemental material.

7. **Experiment statistical significance**

   Question: Does the paper report error bars suitably and correctly defined or other appropriate information about the statistical significance of the experiments?

   Answer: [Yes]

   Justification: Description of significance test and its assumptions are described on Section 6.

   Guidelines:

   - The answer NA means that the paper does not include experiments.

- The authors should answer "Yes" if the results are accompanied by error bars, confidence intervals, or statistical significance tests, at least for the experiments that support the main claims of the paper.
- The factors of variability that the error bars are capturing should be clearly stated (for example, train/test split, initialization, random drawing of some parameter, or overall run with given experimental conditions).
- The method for calculating the error bars should be explained (closed form formula, call to a library function, bootstrap, etc.)
- The assumptions made should be given (e.g., Normally distributed errors).
- It should be clear whether the error bar is the standard deviation or the standard error of the mean.
- It is OK to report 1-sigma error bars, but one should state it. The authors should preferably report a 2-sigma error bar than state that they have a 96% CI, if the hypothesis of Normality of errors is not verified.
- For asymmetric distributions, the authors should be careful not to show in tables or figures symmetric error bars that would yield results that are out of range (e.g. negative error rates).
- If error bars are reported in tables or plots, The authors should explain in the text how they were calculated and reference the corresponding figures or tables in the text.

8. **Experiments compute resources**

   Question: For each experiment, does the paper provide sufficient information on the computer resources (type of compute workers, memory, time of execution) needed to reproduce the experiments?

   Answer: [Yes]

   Justification: It is described in Section A.3.

   Guidelines:

   - The answer NA means that the paper does not include experiments.
   - The paper should indicate the type of compute workers CPU or GPU, internal cluster, or cloud provider, including relevant memory and storage.
   - The paper should provide the amount of compute required for each of the individual experimental runs as well as estimate the total compute.
   - The paper should disclose whether the full research project required more compute than the experiments reported in the paper (e.g., preliminary or failed experiments that didn't make it into the paper).

9. **Code of ethics**

   Question: Does the research conducted in the paper conform, in every respect, with the NeurIPS Code of Ethics `https://neurips.cc/public/EthicsGuidelines`?

   Answer: [Yes]

   Justification: Authors read NeurIPS Code of Ethics and made sure to adhere to it.

   Guidelines:

   - The answer NA means that the authors have not reviewed the NeurIPS Code of Ethics.
   - If the authors answer No, they should explain the special circumstances that require a deviation from the Code of Ethics.
   - The authors should make sure to preserve anonymity (e.g., if there is a special consideration due to laws or regulations in their jurisdiction).

10. **Broader impacts**

    Question: Does the paper discuss both potential positive societal impacts and negative societal impacts of the work performed?

    Answer: [NA]

Justification: The work presented in this paper is a general algorithm for optimizing models trained in a contrastive learning fashion, so there it no direct potential societal impacts. On top of this, we mention how our method requires relatively small training times, reducing the environmental impact. We also mention the dataset medical dataset used in this paper is geographically diverse, but we did not elaborate on that since the model itself is not the main point of the paper. Nevertheless, information abut the countries of origin of the datasets is shown in Appendix A.4

Guidelines:

- The answer NA means that there is no societal impact of the work performed.
- If the authors answer NA or No, they should explain why their work has no societal impact or why the paper does not address societal impact.
- Examples of negative societal impacts include potential malicious or unintended uses (e.g., disinformation, generating fake profiles, surveillance), fairness considerations (e.g., deployment of technologies that could make decisions that unfairly impact specific groups), privacy considerations, and security considerations.
- The conference expects that many papers will be foundational research and not tied to particular applications, let alone deployments. However, if there is a direct path to any negative applications, the authors should point it out. For example, it is legitimate to point out that an improvement in the quality of generative models could be used to generate deepfakes for disinformation. On the other hand, it is not needed to point out that a generic algorithm for optimizing neural networks could enable people to train models that generate Deepfakes faster.
- The authors should consider possible harms that could arise when the technology is being used as intended and functioning correctly, harms that could arise when the technology is being used as intended but gives incorrect results, and harms following from (intentional or unintentional) misuse of the technology.
- If there are negative societal impacts, the authors could also discuss possible mitigation strategies (e.g., gated release of models, providing defenses in addition to attacks, mechanisms for monitoring misuse, mechanisms to monitor how a system learns from feedback over time, improving the efficiency and accessibility of ML).

11. **Safeguards**

    Question: Does the paper describe safeguards that have been put in place for responsible release of data or models that have a high risk for misuse (e.g., pretrained language models, image generators, or scraped datasets)?

    Answer: [NA]

    Justification: We are not releasing any dataset and the downstream tasks trained in this paper does not pose direct risks for misuse.

    Guidelines:

    - The answer NA means that the paper poses no such risks.
    - Released models that have a high risk for misuse or dual-use should be released with necessary safeguards to allow for controlled use of the model, for example by requiring that users adhere to usage guidelines or restrictions to access the model or implementing safety filters.
    - Datasets that have been scraped from the Internet could pose safety risks. The authors should describe how they avoided releasing unsafe images.
    - We recognize that providing effective safeguards is challenging, and many papers do not require this, but we encourage authors to take this into account and make a best faith effort.

12. **Licenses for existing assets**

    Question: Are the creators or original owners of assets (e.g., code, data, models), used in the paper, properly credited and are the license and terms of use explicitly mentioned and properly respected?

    Answer: [Yes]

    Justification: Citations are clear and correct and licenses can be found in Appendix A.4

Guidelines:

- The answer NA means that the paper does not use existing assets.
- The authors should cite the original paper that produced the code package or dataset.
- The authors should state which version of the asset is used and, if possible, include a URL.
- The name of the license (e.g., CC-BY 4.0) should be included for each asset.
- For scraped data from a particular source (e.g., website), the copyright and terms of service of that source should be provided.
- If assets are released, the license, copyright information, and terms of use in the package should be provided. For popular datasets, `paperswithcode.com/datasets` has curated licenses for some datasets. Their licensing guide can help determine the license of a dataset.
- For existing datasets that are re-packaged, both the original license and the license of the derived asset (if it has changed) should be provided.
- If this information is not available online, the authors are encouraged to reach out to the asset's creators.

13. **New assets**

    Question: Are new assets introduced in the paper well documented and is the documentation provided alongside the assets?

    Answer: [Yes]

    Justification: Code and trained models will be released after acceptance with proper documentation.

    Guidelines:

    - The answer NA means that the paper does not release new assets.
    - Researchers should communicate the details of the dataset/code/model as part of their submissions via structured templates. This includes details about training, license, limitations, etc.
    - The paper should discuss whether and how consent was obtained from people whose asset is used.
    - At submission time, remember to anonymize your assets (if applicable). You can either create an anonymized URL or include an anonymized zip file.

14. **Crowdsourcing and research with human subjects**

    Question: For crowdsourcing experiments and research with human subjects, does the paper include the full text of instructions given to participants and screenshots, if applicable, as well as details about compensation (if any)?

    Answer: [NA]

    Justification: This paper does not involve crowd-sourcing nor research with humans since all used datasets already existed.

    Guidelines:

    - The answer NA means that the paper does not involve crowdsourcing nor research with human subjects.
    - Including this information in the supplemental material is fine, but if the main contribution of the paper involves human subjects, then as much detail as possible should be included in the main paper.
    - According to the NeurIPS Code of Ethics, workers involved in data collection, curation, or other labor should be paid at least the minimum wage in the country of the data collector.

15. **Institutional review board (IRB) approvals or equivalent for research with human subjects**

    Question: Does the paper describe potential risks incurred by study participants, whether such risks were disclosed to the subjects, and whether Institutional Review Board (IRB) approvals (or an equivalent approval/review based on the requirements of your country or institution) were obtained?

Answer: [NA]

Justification: We had no study participants since this was an entirely computational work.

Guidelines:

- The answer NA means that the paper does not involve crowdsourcing nor research with human subjects.
- Depending on the country in which research is conducted, IRB approval (or equivalent) may be required for any human subjects research. If you obtained IRB approval, you should clearly state this in the paper.
- We recognize that the procedures for this may vary significantly between institutions and locations, and we expect authors to adhere to the NeurIPS Code of Ethics and the guidelines for their institution.
- For initial submissions, do not include any information that would break anonymity (if applicable), such as the institution conducting the review.

16. **Declaration of LLM usage**

Question: Does the paper describe the usage of LLMs if it is an important, original, or non-standard component of the core methods in this research? Note that if the LLM is used only for writing, editing, or formatting purposes and does not impact the core methodology, scientific rigorousness, or originality of the research, declaration is not required.

Answer: [NA]

Justification: No LLM was used beyond rephrasing in the making of this paper.

Guidelines:

- The answer NA means that the core method development in this research does not involve LLMs as any important, original, or non-standard components.
- Please refer to our LLM policy (`https://neurips.cc/Conferences/2025/LLM`) for what should or should not be described.